EHD2-mediated restriction of caveolar dynamics regulates cellular lipid uptake

Claudia Matthäus[1,9*], Ines Lahmann[2,9], Séverine Kunz[3], Wenke Jonas[4], Arthur Alves Melo[1], Martin Lehmann[5], Elin Larsson[6], Richard Lundmark[6,10], Volker Haucke[5,10], Dominik N. Müller[7,10], Annette Schürmann[4,10], Carmen Birchmeier[2,10], Oliver Daumke[1,8,10,11*]

[1] Crystallography, Max-Delbrück-Center for Molecular Medicine, Berlin, Germany

[2] Signal Transduction/Developmental Biology, Max-Delbrück-Center for Molecular Medicine, Berlin, Germany

[3] Electron Microscopy Facility, Max-Delbrück-Center for Molecular Medicine, Berlin, Germany

[4] Experimental Diabetology, German Institute of Human Nutrition, German Center for Diabetes Research, München-Neuherberg, Potsdam, Germany

[5] Dept. of Molecular Pharmacology & Cell Biology and Imaging Core Facility, Leibniz-Forschungsinstitut für Molekulare Pharmakologie, Berlin, Germany

[6] Integrative Medical Biology, Umeå University, 901 87 Umeå, Sweden

[7] Experimental & Clinical Research Center, a cooperation between Charité Universitätsmedizin Berlin and Max Delbrück Center for Molecular Medicine, Berlin, Germany

[8] Institute of Chemistry and Biochemistry, Freie Universität Berlin, Takustrasse 6, 14195 Berlin, Germany
Lead contact

[9] These authors contributed equally

[10] Senior author

[11] Lead contact

*Corresponding authors

Correspondence: claudia.matthaeus@mdc-berlin.de; oliver.daumke@mdc-berlin.de

Abstract

Eps15-homology domain containing protein 2 (EHD2) is a dynamin-related ATPase located at the neck of caveolae, but its physiological function has remained unclear. We found that global genetic ablation of EHD2 in mice led to increased fat deposits in several organs. This organismic phenotype was paralleled at the cellular level by an increased lipid uptake via a CD36-dependent pathway, an elevated number of detached caveolae and higher caveolar mobility. Following a high fat diet, various enzymes involved in *de novo* fatty acid synthesis were down-regulated in EHD2 KO mice. Furthermore, EHD2 expression itself was down-regulated in the visceral fat of two obese mouse models and in diet-induced obesity. Thus, EHD2 controls a cell-autonomous, caveolae-dependent lipid uptake pathway, implicating a role of EHD2 in fat accumulation and obesity.

Keywords: EHD proteins, caveolae, fatty acid uptake, CD36, lipid metabolism, obesity

48 **Introduction**

49 Caveolae are small membrane invaginations of the plasma membrane that are abundantly found
50 in adipocytes, endothelial and muscle cells (Cheng and Nichols, 2016). They have been implicated in the
51 regulation of membrane tension (Sinha *et al.*, 2011; Torrino *et al.*, 2018), in mediating lipid metabolism
52 (Liu *et al.*, 2008), or in acting as distinct sites for specific and highly regulated signaling cascades such as
53 the endothelial nitric oxide synthase (eNOS)-nitric oxide (NO) pathway (Ju *et al.*, 1997). The
54 characteristically shaped caveolar bulb has a typical diameter of 50 - 100 nm and is connected to the cell
55 surface via a narrow neck region. The integral membrane protein Caveolin (with three isoforms in human,
56 Cav1-3) and the peripheral membrane protein Cavin (with four isoforms in human, Cavin1-4) build a mesh-
57 like coat around the caveolar bulb (Ludwig *et al.*, 2013; Kovtun *et al.*, 2015; Mohan *et al.*, 2015; Ludwig,
58 Nichols and Sandin, 2016; Stoeber *et al.*, 2016). In addition, BAR domain containing proteins of the
59 PACSIN/syndapin family (PACSIN1-3 in human) participate in the biogenesis of caveolae (Hansen, Howard
60 and Nichols, 2011; Senju *et al.*, 2011; Seemann *et al.*, 2017).

61 Loss of Cav1/Cav3 or Cavin1 results in a complete lack of caveolae from the plasma membrane
62 (Drab *et al.*, 2001; Hill *et al.*, 2008; Liu *et al.*, 2008). Also, Cavin2 knockout (KO) mice show a decreased
63 number of caveolae at the plasma membrane in adipocytes and lung endothelium, but not in
64 cardiomyocytes or heart endothelium, suggesting a cell-type specific function (Hansen *et al.*, 2013). In
65 contrast, loss of the muscle-enriched PACSIN3/syndapin III leads to the loss of caveolae in cardiomyocytes
66 (Seemann *et al.*, 2017). The deletion of Cavin3 alone does not alter caveolae formation or caveolar protein
67 assembly (Hansen *et al.*, 2013; Liu *et al.*, 2014).

68 Cav1 KO mice suffer from cardiomyopathy, pulmonary hypertension, endothelium-dependent
69 relaxation problems and defective lipid metabolism (Cheng and Nichols, 2016). In agreement with the
70 latter, Cav1 KO mice are resistant to high fat diet-induced obesity (Razani *et al.*, 2002) and display smaller
71 white adipocytes and fat pads (Martin *et al.*, 2012). Furthermore, increased levels of triglycerides and fatty

72 acids are found in blood plasma samples obtained from Cav1 KO mice suggesting a reduced cellular uptake
73 of fatty acids (Razani *et al.*, 2002). A similar metabolic phenotype was found in mice lacking Cavin1 (Hill *et*
74 *al.*, 2008; Liu *et al.*, 2008; Ding *et al.*, 2014). Conversely, overexpression of Cav1 in adipocytes results in
75 enhanced fat accumulation, enlarged adipocytes and lipid droplets (LDs) (Briand *et al.*, 2014). An increased
76 number of caveolae is also found at the plasma membrane of Cav1 overexpressing adipocytes. These
77 results suggest that caveolae are involved in fat accumulation in adipocytes and may promote fatty acid
78 uptake (Pohl *et al.*, 2004). However, the molecular mechanisms of caveolae-dependent fat uptake have
79 remained obscure.

80 Eps15 homology domain containing protein 2 (EHD2) localizes to the caveolar neck region (Morén
81 *et al.*, 2012; Stoeber *et al.*, 2012; Ludwig *et al.*, 2013). The protein belongs to the dynamin-related EHD
82 ATPase family, which comprises four members in human (EHD1-4), and shows strong expression in human
83 adipose and muscle tissue (human protein atlas) (Uhlén *et al.*, 2015). EHD is built of an N-terminal GTPase
84 (G)-domain, which mediates dimerization and oligomerization, a helical domain containing the membrane
85 binding site, and a C-terminal regulatory Eps15 homology (EH)-domain. The proteins exist in a closed auto-
86 inhibited conformation in solution (Daumke *et al.*, 2007). When recruited to membranes, a series of
87 conformational changes aligns the phospholipid binding sites with the membrane and facilitates
88 oligomerization of EHD2 into ring-like structures (Shah *et al.*, 2014; Hoernke *et al.*, 2017; Melo *et al.*,
89 2017).

90 Down-regulation of EHD2 in cell culture results in decreased surface association and increased
91 mobility of caveolae, whereas EHD2 overexpression stabilizes caveolae at the plasma membrane (Morén
92 *et al.*, 2012; Stoeber *et al.*, 2012; Mohan *et al.*, 2015; Shvets *et al.*, 2015). This led to the hypothesis that
93 formation of an EHD2-ring at the neck of caveolae restricts caveolar mobility within the membrane. In
94 agreement with this hypothesis, EHD2 assembles in an ATP-dependent fashion into ring-like oligomers *in*
95 *vitro* and induces the formation of tubular liposomes with an inner diameter of 20 nm, corresponding to

96 the diameter of the caveolar neck (Daumke et al., 2007). Whether EHD2 also controls caveolar membrane
97 dynamics *in vivo* and what the physiological consequences of EHD2 loss at the organismic level are, is
98 unknown.

99 In this study, we found that EHD2 KO mice revealed enlarged fat accumulations in several organs,
100 and increased lipid droplets (LDs) in caveolae-harboring cell types like adipocytes, muscle or liver cells. In
101 tissue and cells lacking EHD2, caveolae were frequently detached from the plasma membrane and
102 displayed elevated mobility. We demonstrate that fatty acid uptake via the fatty acid translocase CD36 is
103 increased in adipocytes from EHD2 KO mice. Furthermore, in two obesity mouse models or after high fat
104 diet, reduced EHD2 expression and an increased numbers of detached caveolae were found in visceral fat.
105 Our data establish EHD2 as a negative regulator of caveolae-dependent lipid uptake and implicate a crucial
106 role of caveolar stability and dynamics for lipid homeostasis and obesity.

107

108 **Results**

109 **Generation of EHD2 knockout mouse model**

110 To elucidate the expression pattern of EHD2, immunostainings on cryostat sections of C57BL6/N
111 E15 mouse embryos were performed. They revealed strong EHD2 expression in the developing heart (Fig.
112 1A, see arrow), blood vessels (Fig. 1A, e.g. umbilical cord marked by star) and brown adipose tissue (BAT,
113 Fig. 1A, see arrow head), e.g. in tissues where caveolae are particularly abundant (Cheng and Nichols,
114 2016). These results were corroborated by *in situ* hybridizations against EHD2 mRNA, which indicated
115 strong EHD2 expression in BAT of an E18 C57BL6/N embryo (Fig. S1A). Intense EHD2 staining was also
116 observed in cryostat sections of adult C57BL6/N heart, white adipocyte tissue (WAT) and BAT (Fig. 1B-D).

117 To examine the physiological function of EHD2, a mouse strain with LoxP recognition sites
118 surrounding exon 3 and intron 3 of the *Ehd2* gene was engineered (Fig. 1E). Exon 3 encodes part of the
119 highly conserved GTPase domain (residues 137-167), and its deletion is predicted to result in non-

120 functional protein. Following global removal of exon 3 by crossings with a germ-line specific Cre-deleter
121 strain, offspring mice were back-crossed with the C57BL6/N mouse strain for five generations, yielding a
122 global EHD2 KO mouse model.

123 Genotyping of offspring confirmed the successful deletion of EHD2 exon 3 in EHD2 del/del animals
124 (Fig. 1F) and real-time PCR revealed the absence of EHD2 mRNA in the EHD2 del/del tissue (Fig. 1G).
125 Western blot analysis of EHD2 +/+ and del/+ tissues indicated the expression of EHD2 in several organs,
126 such as heart, muscle, fat, lung, intestine and bladder, compared to its complete loss in EHD2 del/del mice
127 (Fig. 1H). Cav1 and Cavin1 protein levels remained unchanged upon loss of EHD2. Immunostaining of
128 cryostat sections obtained from EHD2 del/del brown adipose tissue did not reveal any significant
129 differences in Cav1 or Cavin1 expression and localization (Fig. S1B). Furthermore, BAT immunostainings
130 in adult mice illustrated the same high expression of EHD2 for +/+ and del/+ mice, whereas the EHD2 KO
131 mice (del/del) showed a complete loss of EHD2 staining (Fig. 1I). In adult heart sections, specific staining
132 of EHD2 in +/+ and del/+ mice was observed, and again no staining was seen in EHD2 KO mice (Fig. S1C).
133

134 **Loss of EHD2 results in increased lipid accumulation**

135 EHD2 del/del mice were born in normal Mendelian ratios, were fertile and did not show an
136 obvious phenotype upon initial inspection. However, when one year-old EHD2 del/del male mice were
137 dissected, the heart was surrounded by white fat deposits, and an increased amount of epigonadal and
138 periinguinal white fat was observed, in contrast to the EHD2 del/+ male sibling controls or C57BL6/N male
139 mice (Fig. 2A, C, Fig. S2A). Notably, heart and body weight did not differ in EHD2 del/del compared to
140 EHD2 del/+ mice (Fig. 2B-D).

141 When analyzed in more detail, white adipocytes of EHD2 del/del mice showed an increased cell
142 size compared to adipocytes of EHD2 del/+ mice (Fig. 2E, F), likely due to increased lipid storage. Indeed,
143 lipid composition measurements of WAT indicated an increased amount of storage lipids (mainly

144 triacylglycerol) in EHD2 del/del mice compared to EHD2 del/+ (Fig. 2G). Similarly, elevated fat
145 accumulations in LDs were found in EHD2 del/del BAT (Fig. 2H). Histological inspections of BAT paraffin
146 and cryostat sections stained against the LD coat protein Perilipin1 indicated an increased LD size in EHD2
147 del/del BAT compared to EHD2 del/+ or C57BL6/N mice (Fig. 2I, J, Fig. S2B-D). Moreover, liver of EHD2
148 del/del mice displayed a yellowish appearance, suggesting increased fat accumulation (Fig. 2K). This was
149 confirmed by Oil red O staining of liver sections (Fig. 2L, Fig. S2E). Elevated fat accumulations were also
150 observed in EHD2 del/del muscle sections (Fig. 2L, M, Fig. S2E, F), indicating a general function of EHD2 in
151 lipid metabolism in many cell types. As no significant differences in EHD2 expression levels and lipid
152 accumulation (Fig. 1, S1 and S2) were found in EHD2 del/+ and C57BL6/N male mice, the following animal
153 experiments were carried out with EHD2 del/+ as control group to EHD2 del/del male mice to reduce
154 animal numbers.

155 Based on the increased lipid accumulation in EHD2-lacking adipocyte tissue, we further
156 investigated if adipocyte differentiation is impaired in EHD2 del/del WAT. However, gene expression
157 analysis of adipogenic marker genes like PPRaγ, Retn or Serpina3k displayed no significant change
158 compared to EHD2 del/+ WAT (Fig. S2G). Furthermore, glucose tolerance was tested in EHD2 del/del mice
159 but did not reveal major differences for blood glucose concentrations after glucose injection compared to
160 EHD2 del/+ mice (Fig. S2H).

161

162 **Increased lipid droplet size in adipocytes lacking EHD2**

163 To explore the function of EHD2 at the cellular level, lipid metabolism was investigated in cultured
164 adipocytes. Primary pre-adipocytes were isolated from WAT of EHD2 del/+ and EHD2 del/del mice and
165 differentiated into mature adipocytes. Oil red O staining revealed increased lipid accumulation in
166 adipocytes lacking EHD2 (Fig. 3A, B). BODIPY staining of these cultures was used to measure the LD size.
167 Undifferentiated EHD2 del/+ and del/del pre-adipocytes had similarly sized LDs. In contrast, enlarged LDs

168 were found in differentiated EHD2 del/del adipocytes, compared to a moderate size increase in EHD2
169 del/+ cells (Fig. 3C-E). 3D reconstruction of EHD2 del/del differentiated adipocytes revealed that some LDs
170 even exceeded the volume of the nucleus (Fig. 3C).

171 Next, we aimed to address the possibility that increased lipid uptake is a secondary effect of EHD2
172 deletion mediated via putative organ cross-talk. We therefore repeated the experiments with cultivated
173 adipocytes derived from EHD2 cKO flox/flox mice, in which EHD2 expression was down-regulated by
174 expression of Cre recombinase via viral transfection (AAV8). Again, EHD2 removal led to increased LD
175 growth (Fig. 3F), indicating a cell-autonomous function of EHD2 in controlling lipid uptake.

176 LD growth is mainly mediated by extracellular fatty acid uptake and conversion into triglycerides,
177 whereas increased glucose uptake and *de novo* lipogenesis only play a minor role in this process (Wilfling
178 *et al.*, 2013; Rutkowski, Stern and Scherer, 2015). Fatty acids and lipids are present in high concentrations
179 in fetal bovine serum (FBS). Addition of delipidated FBS during adipocyte differentiation resulted in
180 complete loss of LD in both genotypes (Fig. 3G), whereas glucose-depletion led to a general impairment
181 of adipocyte differentiation. However, enlarged LD could still be observed in KO adipocytes under the
182 latter conditions (Fig. 3G). These data led us to speculate that the increased LD size in EHD2 del/del
183 adipocytes may be a consequence of increased fatty acid uptake.

184 To test this possibility directly, we monitored the uptake of extracellularly added fatty acids into
185 differentiated adipocytes using BODIPY-labelled dodecanoic acid (FA12) paired with FACS analysis. After
186 5 min, only a minor fraction of EHD2 del/+ adipocytes displayed intense BODIPY staining (R2, for definition
187 see Fig. 3H, J). This R2 population increased to more than 30% after 60 min of FA12 treatment. EHD2
188 del/del adipocytes displayed increased BODIPY staining at both early (Fig. 3I, K) and late time points (Fig.
189 3I, L), indicating accelerated lipid uptake. In line with these experiments, light microscopy imaging
190 revealed a more intense BODIPY staining of EHD2 del/del cells compared to EHD2 del/+ adipocytes after
191 60 min of fatty acid incubation (Fig. 3M). In contrast, EHD2 del/+ and EHD2 del/del adipocytes did not

192 differ with respect to their ability to take up extracellularly added glucose (Fig. S3A-C). Previously, an
193 involvement of EHD2 in the autophagic engulfment of LD (lipophagy) was suggested (Li *et al.*, 2016).
194 However, inducing starvation by incubation of differentiated adipocytes with Hank's balanced salt
195 solution (HBSS) revealed no differences in the release of stored lipids in EHD2 del/+ and EHD2 del/del
196 adipocytes, and both genotypes displayed similar reductions in lipid accumulation (Fig. S3D). These data
197 indicate that loss of EHD2 does not affect the release of fatty acids or lipophagy, but specifically controls
198 LD size by regulating fatty acid uptake.
199
200 **Loss of EHD2 results in detachment of caveolae from the plasma membrane *in vivo***
201 To address if the absence of EHD2 results in altered caveolar morphology, WAT and BAT were
202 analyzed by electron microscopy (EM). Caveolae in EHD2 del/+ BAT were mostly membrane-bound and
203 displayed the characteristic flask-shaped morphology (Fig. 4A, white arrows, ratio detached/membrane
204 bound caveolae = 0.27). Strikingly, an increased number of caveolae were detached from the plasma
205 membrane in BAT isolated from EHD2 del/del mice compared to EHD2 del/+ controls (Fig. 4A, B, black
206 arrows, ratio detached/membrane bound caveolae = 1.75). The total number of caveolae, as well as the
207 caveolar diameter and size, were unchanged in brown adipocytes lacking EHD2. An increased number of
208 detached caveolae were also observed in EHD2 del/del white adipocytes compared to EHD2 del/+ cells
209 from littermate controls (Fig. 4C, D, black and white arrow heads, ratio detached/membrane bound
210 caveolae (del/del) = 1.2 vs. ratio (del/+) = 0.24). In white adipocytes, a reduced total number of caveolae
211 was determined, while both caveolar size and diameter were increased in EHD2 del/del compared to EHD2
212 del/+ animals (Fig. 4D). Cav1 immunogold labeling confirmed that the round vesicles close the plasma
213 membrane, indeed, were detached caveolae (Fig. 4E). 3D visualization of EHD2 del/del brown adipocyte
214 by electron tomography (ET) further demonstrated that the majority of detached caveolae in 2D EM
215 images were not connected to the plasma membrane (Fig. 4F, G, Movie S1) but localized 20-30 nm

216 underneath (Fig. 4G a, b), although some caveolae close to the plasma membrane showed thin
217 connections (Fig. 4G b, d, white arrow head). Taken together, EM and ET reveal an increased detachment
218 of caveolae from the plasma membrane in EHD2 del/del adipocytes, suggesting a crucial function for EHD2
219 in the stabilization of caveolae at the plasma membrane.
220
221 **Increased caveolar mobility in EHD2 knockout cells**
222 To verify the cell-autonomous EHD2-mediated control of LD size and to further dissect the
223 interplay of caveolar mobility and LD growth at the molecular level, we analyzed mouse embryonic
224 fibroblasts (MEFs) derived from EHD +/+ and EHD2 del/del mice. Oil Red O staining showed increased
225 intensity in EHD2 del/del MEFs after adipogenic differentiation compared to EHD2 +/+ MEFs (Fig. S4A),
226 suggesting increased lipid accumulation. BODIPY staining of EHD2 del/del MEFs revealed enlarged LD sizes
227 after differentiation or treatment with oleic acid for 6 h (Fig. S4B, C). Furthermore, both storage and
228 membrane lipids were largely increased in MEFs lacking EHD2 (Fig. S4D). Re-expression of an EGFP-tagged
229 EHD2 version in MEFs lacking EHD2 completely rescued the observed LD phenotype. In fact,
230 overexpression of EHD2 in +/+ and del/del MEFs reduced the size of LDs compared to EGFP expressing
231 cells (Fig. 5A, B). These data indicate a general and cell autonomous role of EHD2 in the control of LD
232 growth and size.
233 To test if the observed increased LD size in EHD2 del/del MEFs was dependent on caveolae, MEFs
234 lacking EHD2 were treated with Cav1 siRNA to eliminate caveolae. Indeed, LD sizes in EHD2 KO MEFs were
235 significantly decreased after Cav1 knockdown compared to control siRNA treated cells (Fig. 5C, D),
236 pointing to a crucial role of caveolae in EHD2-controlled LD size.
237 Next, we investigated caveolar mobility and endocytosis of Cholera toxin subunit B (CTxB) in EHD2
238 +/+ and del/del MEFs. CTxB can be internalized by multiple pathways including caveolar uptake as well as

239 by clathrin-(and caveolin)-independent carriers (CLICs, Parton and Simons et al., 2007). Strikingly, MEFs
240 lacking EHD2 showed increased CTxB uptake compared to EHD2 +/+ MEFs (Fig. 5E, F).

241 To analyze caveolae dynamics directly, we monitored caveolar movement by total internal
242 reflection fluorescence (TIRF) microscopy. EHD2 +/+ and del/del MEFs were transfected with pCav1-EGFP
243 to label single caveolae. As illustrated in Fig. 5G, regions of moderate Cav1 expression were investigated
244 to ensure that distinct Cav1 spots were observed during the analysis. Live TIRF imaging of EHD2 wt MEFs
245 showed a slow or no continuous movement for the majority of investigated caveolae (Movie S2).
246 However, single caveolae moved along the plasma membrane or left the TIRF illumination zone towards
247 the inside of the cell, indicative of their spontaneous detachment, as previously reported (Moren et al.,
248 2012). Strikingly, movement and velocity of caveolae was greatly increased in EHD2 del/del MEFs (Movie
249 S3), not allowing Cav1 single spots to be tracked. Line scan analysis revealed a greatly reduced number of
250 fixed, non-moving Cav1 spots (referred to as lines in Fig. 5G) in EHD2 del/del MEFs compared to wt cells.
251 Moreover, a larger number of highly mobile Cav1 sparks, reflecting fast moving caveolae, was found in
252 EHD2 del/del cells (Fig. 5G, H). Re-expression of EHD2 in EHD2 del/del MEFs reduced the mobility of
253 caveolae, often leading to their immobilization (Fig. S4E). Collectively, these data show that EHD2 crucially
254 regulates cellular lipid uptake and caveolar mobility.

255

256 **The fatty acid translocase CD36 is involved in EHD2-dependent fatty acid uptake**

257 CD36 had previously been implicated in caveolae-dependent fatty acid uptake (Aboulaich *et al.*,
258 2004; Ring *et al.*, 2006; Eyre *et al.*, 2007). We therefore examined whether the increased fatty acid uptake
259 in EHD2 del/del adipocytes and EHD2 del/del MEFs is mediated by CD36. Initially, we analyzed CD36
260 localization in MEFs using immuno-live stainings (Fig. 6A). Strong CD36 signal was detected at the cell
261 membrane, where a minor pool of CD36 co-localized with Cav1. Partial co-localization of CD36 and Cav1
262 was further confirmed by high-resolution z-stack imaging (Fig. 6A). Both EHD2 KO MEFs (Fig. 6A) and

263 del/del adipocytes (Fig. S4F) showed a slight reduction in CD36 plasma membrane levels compared to
264 EHD2 expressing cells (Fig. 6C, siRNA negative control), possibly reflecting the increased amount of
265 detached caveolae due to EHD2 loss. Removal of caveolae by Cav1-specific siRNAs treatment resulted in
266 significantly decreased CD36 plasma membrane staining in EHD2 +/+ and del/del MEFs (Fig. 6B, C)
267 suggesting a function of caveolae for CD36 membrane localization (Fig. 6D).

268 To investigate the causal relationship between the increased LD growth in EHD2 KO MEFs and
269 CD36-mediated lipid uptake, CD36 expression was downregulated in MEFs by treatment with either one
270 of three specific CD36 siRNA, followed by oleic acid application and LD staining. CD36 antibody staining
271 confirmed efficient knockdown of CD36 in EHD2 +/+ and del/del MEFs (Fig. 6E). Strikingly, removal of
272 CD36 in EHD2 +/+ and del/del MEFs dramatically decreased the size of LDs compared to a control siRNA
273 treated cells (Fig. 6E, F). We conclude that the observed enlargement of LDs in cells lacking EHD2 depends
274 on CD36.

275

276 **Decreased EHD2 expression in genetic obesity models or diet induced obesity**

277 To examine the effect of genetic EHD2 deletion during diet-induced obesity, EHD2 del/+ and
278 del/del mice were fed with a high fat diet (60% kcal fat) for 10 days or 4 months, and the body weight was
279 monitored every 5 days.

280 Within the first 10 days of high fat feeding, a strong rise in body weight was observed for both
281 genotypes, which was slightly faster in EHD2 del/del mice compared to EHD2 del/+ (Fig. 7A, 0.84 vs. 0.73
282 g/day). However, in the following days, the differences in the overall body weight disappeared (Fig. 7B).
283 As already observed in EHD2 del/del mice on a standard diet, white and brown adipocytes from EHD2
284 del/del mice revealed enlarged LD sizes compared to EHD2 del/+ after 10 days on the high fat diet (Fig.
285 7D). Similar effects were obtained in liver sections (Fig. 7D). After 4 months of high fat feeding, enlarged

286 lipid accumulation was observed in adipocytes and liver in both genotypes (Fig. S5A, B). Fat mass in EHD2
287 del/+ and EHD2 del/del mice did not differ after short or long-term high fat feeding (Fig. 7C).
288 The weight adaptation of both genotypes suggested the occurrence of compensatory
289 mechanisms. First, we looked for changes of adiponectin, leptin and insulin blood levels but did not detect
290 any significant difference in mice lacking EHD2 compared to EHD2 del/+ mice after 4 months of high fat
291 feeding or under standard diet (Fig. S6A, B). Free fatty acid concentration in blood plasma was slightly
292 reduced in EHD2 del/del samples after standard diet indicating increased fatty acid uptake (Fig. S6B).
293 Already under standard diet, we observed a down-regulation of genes involved in *de novo*
294 lipogenesis in EHD2 del/del vs. EHD2 del/+ mice (Fig. 7E). Similar results were obtained for primary
295 adipocyte cell cultures (Fig. S3E). High fat diet led to a drastic reduction of gene expression in *de novo*
296 lipogenesis like SREBP1 and FAS in WAT obtained from EHD2 del/del mice, suggesting that downregulation
297 of lipogenesis is an active mechanism that partially compensates for the enhanced lipid uptake (Fig. 7F).
298 Remarkably, EHD2 expression was essentially absent in WAT obtained from EHD2 del/+ mice following a
299 4 months high fat diet (Fig. 7G). This may explain the similar phenotypes of EHD2 del/+ and EHD2 del/del
300 mice following a long-term high fat diet (Fig. 7B, Fig. S5).
301 Based on these observations, EHD2 expression was investigated in two obesity-related mouse
302 models, ob/ob and NZO (Kleinert *et al.*, 2018). Indeed, WAT obtained from ob/ob and NZO mice showed
303 reduced EHD2 expression compared to C57BL6/N mice fed by standard diet (Fig. 7H). When investigating
304 adipocytes from ob/ob mice, a higher proportion of detached caveolae were found in the obesity mouse
305 model (ratio detached/membrane bound caveolae = 1.4 vs. 0.35 in C57BL6/N mice fed with standard diet,
306 Fig. 7I-J). Taken together, these data indicate that EHD2 expression is highly regulated by lipid uptake and
307 load and suggest that EHD2-mediated caveolar dynamics is altered in obesity.
308
309 **Discussion**

310 Here, we identify EHD2 as a negative regulator of caveolae-dependent lipid uptake. In caveolae
311 containing cells, like adipocytes, muscle cells or fibroblasts, loss of EHD2 resulted in increased lipid
312 accumulation, which was observed in the whole organism as well as in cell culture-based experiments.
313 Loss of EHD2 was associated with the detachment of caveolae from the plasma membrane, higher
314 caveolar mobility and increased uptake of lipids and other caveolar substrates, such as CTxB. We
315 demonstrate that the fatty acid translocase CD36 participates in this EHD2-dependent lipid uptake
316 pathway. Furthermore, obese mouse models and mice exposed to a long-term high fat diet exhibit
317 decreased EHD2 expression in WAT. Thus, our study reveals a cell-autonomous lipid uptake route that
318 involves CD36 and caveolae, is controlled by EHD2 and modified by metabolic conditions.

319 For some time, caveolae have been implicated in lipid uptake. Thus, mice lacking caveolae showed
320 reduced fat mass and did not develop any form of obesity. In addition, Pohl et al. (2005) observed
321 decreased oleate uptake after expression of a dominant-negative Cav1 mutant. The EHD2 KO mouse
322 model, described here, revealed the opposite phenotype, e.g. a caveolae gain-of-function *in vivo* model.
323 In EHD2 KO mice, caveolae were more often detached from the plasma membrane and showed a higher
324 mobility and faster lipid uptake, resulting in enlarged LDs. Unlike in Cav1 over-expressing mice (Briand *et*
325 *al.*, 2014), which also show increased fatty acid uptake, the number of caveolae remained unchanged in
326 EHD2 KO mice. This supports a model in which not only caveolae numbers, but also caveolar dynamics
327 play a crucial role in this process (see model in Fig. 7K). Furthermore, such idea is in line with our structural
328 findings that EHD2 can form ring-like oligomers that may stabilize the neck of caveolae (Daumke et al,
329 2007; Shah et al., 2014; Melo et al., 2017; Hoernke et al., 2017), thereby restricting caveolar mobility
330 (Morén *et al.*, 2012; Stoeber *et al.*, 2012). Based on studies in EHD2 KO NIH 3T3 cell line, Yeow et al. (2017)
331 suggested that EHD1 and/or EHD4 could rescue loss of EHD2 during its role in membrane protection.
332 However, we did not find rescue of caveolae detachment and lipid uptake in EHD2 KO cells by other EHD
333 family members.

334 We show that CD36 partially co-localizes with caveolae and is involved in EHD2-mediated lipid
335 uptake. Previous Cav1 KO studies already showed mis-localization of CD36 and impaired fatty acid uptake
336 in MEFs lacking caveolae (Ring *et al.*, 2006). CD36 belongs to a superfamily of integral membrane protein,
337 the CD36 scavenger receptors, which also include the lysosomal integral membrane protein II (LIMP 2).
338 The structure of the latter revealed a large hydrophobic tunnel in the conserved globular domain which
339 was suggested to deliver lipids in the outer membrane (Hsieh *et al.*, 2016). The specific lipid environment
340 of caveolae, including a high proportion of cholesterol, may support CD36-mediated lipid uptake in
341 caveolae. Our data support the idea that caveolae shuttling between the plasma membrane and
342 intracellular compartments is involved in lipid uptake (as illustrated in Fig. 7K). Conventional caveolae
343 internalization follows the endosomal pathway from early to late endosomes and finally to lysosomes
344 (Pelkmans *et al.*, 2004; Hayer *et al.*, 2010). However, initial cellular fatty acid accumulation within LDs can
345 be much faster (minutes) (Kuerschner, Moessinger and Thiele, 2008) compared to the caveolar turnover
346 in lysosomes (one hour), suggesting an involvement of alternative pathways. Notably, LDs form at the
347 membrane of the endoplasmic reticulum (ER) (Pol, Gross and Parton, 2014; Wilfling *et al.*, 2014; Barneda
348 and Christian, 2017), and it was proposed before that caveolae could translocate to the ER and form
349 contact sites (Le *et al.*, 2002; Le, 2003). Furthermore, a role of Cav1 in LD formation has been suggested
350 (Ostermeyer *et al.*, 2001; Schlegel, Arvan and Lisanti, 2001; Robenek *et al.*, 2004). With the EHD2 KO mice,
351 we have developed a suitable model to explore the molecular components of the caveolae-dependent
352 lipid uptake pathway.

353 The loss of EHD2 on the cellular level led to increased fat deposits on the organismic level, which
354 was particularly evident in older animals. The observed phenotype based on the global loss of EHD2 could
355 be influenced by organ-organ interactions (Stern, Rutkowski and Scherer, 2016). However, we did not find
356 any evidence for differences in adipocyte derived secretory factors, such as adiponectin (Fig. S6).
357 Furthermore, increased lipid uptake was dependent on caveolae, as shown by Cav1 knockdown

358 experiments, and lipid droplet growth could specifically be induced by viral transfection of Cre
359 recombinase in EHD2 cKO flox/flox, but not in flox/wt adipocytes. Thus, increased lipid uptake is caused
360 by a cell-autonomous, caveolae-dependent mechanism. As the WAT distribution and lipid accumulation
361 is known to differ in male and female mice, further studies are required to analyze potential sex-specific
362 differences in EHD2-dependent lipid uptake.

363 Despite the observed LD accumulation in mice lacking EHD2 (under standard and high fat diet),
364 the body weight and overall fat mass of EHD2 del/del and EHD2 del/+ mice were not altered, suggesting
365 metabolic compensation. In line with this idea, EHD2 del/del WAT and cultivated EHD2 del/del adipocytes
366 showed a significant reduction in expression levels of genes involved in *de novo* lipogenesis like SREBP1
367 or FAS indicating a strong downregulation of glucose-dependent fatty acid production in fat cells. Similar
368 compensatory mechanisms were noted in patients suffering from obesity (Eissing *et al.*, 2013; Guiu-Jurado
369 *et al.*, 2015; Solinas, Borén and Dulloo, 2015). Even with elevated fat content in the adipose tissues, liver
370 and skeletal muscle EHD2 del/del mice did not develop an insulin resistance as indicated by the normal
371 glucose tolerance.

372 Remarkably, the expression levels of EHD2 in WAT of two obese mouse models (ob/ob and NZO
373 mice) and of EHD2 del/+ mice treated with a long-term high fat diet were significantly lower than in
374 C57BL6/N or EHD2 del/+ mice under standard diet, resulting in detachment of caveolae. Thus, expression
375 of EHD2 appears to negatively correlate with adipocyte size, therefore reflecting the situation in the EHD2
376 KO mouse (see also (Sonne *et al.*, 2017)). Consistent with this observation, it was previously reported that
377 increased Cav1 expression and caveolae number were detected in patients suffering from obesity or T2D,
378 and also in obesity rat models (Catalán *et al.*, 2008; Grayson *et al.*, 2013). We speculate that an imbalance
379 in number, life-time and mobility of caveolae appears to accompany and maybe actively contribute to the
380 development and progression of obesity. Accordingly, pharmacological approaches to enhance EHD2

381 expression or its stabilization at the plasma membrane could reduce lipid uptake and consequently help
382 to treat obesity in patients.
383 In conclusion, our study reveals a conserved cellular lipid uptake pathway that involves caveolae
384 and CD36 and is controlled by EHD2.
385

386 **Acknowledgments**

387 We thank Petra Stallerow for taking care of the EHD2 delta E3 mouse strain, Karin Jacobi for advice with
388 the animal application, Arnd Heuser and the pathophysiology facility for measuring the body composition,
389 Vivian Schulz for helping with the genotyping of the mice, Claudio Shah for purifying the EHD2 antiserum,
390 and the advanced light imaging facility at MDC for technical support. The authors acknowledge financial
391 support from the Deutsche Forschungsgemeinschaft (DFG; SFB 958/A7 to V.H., A12 to O.D., A13 to A.S.)
392 and support by The Initiative and Networking Fund of the Helmholtz Association.
393

394 **Author Contributions**

395 C.M. planned, performed and analyzed all experiments if not otherwise indicated. C.M. and O.D. wrote
396 the manuscript, with input from all authors. S.K. performed and analyzed all EM imaging, C.M. analyzed
397 EM images, S.K. and C.M. performed and analyzed ET. I.L. generated the EHD2 KO mouse model and
398 performed in situ hybridization. W.J. analyzed blood plasma markers and EHD2 expression in obesity
399 mouse models. M.L. helped during TIRF imaging and discussed experiments, A.M. isolated primary MEF
400 and performed the EHD2 Western Blot. E.L. performed lipid droplet staining experiments after Cav1
401 knockdown. A.S., V.H., R.L., C.B. and D.N.M. discussed potential experiments and the manuscript. O.D.
402 wrote the mouse animal application with help of D.N.M. and C.M.
403

404 **Declaration of Interests**

405 The authors declare no competing interests.

406

407 **References**

408 Aboulaich, N., Vainonen, J. P., Stralfors, P. and Vener, A. V (2004) 'Vectorial proteomics reveal targeting,
409 phosphorylation and specific fragmentation of polymerase I and transcript release factor (PTRF) at the
410 surface of caveolae in human adipocytes.', *The Biochemical journal*, 383(Pt 2), pp. 237–48. doi:
411 10.1042/BJ20040647.

412 Barneda, D. and Christian, M. (2017) 'Lipid droplet growth: regulation of a dynamic organelle', *Current*
413 *Opinion in Cell Biology*. Elsevier Ltd, 47, pp. 9–15. doi: 10.1016/j.ceb.2017.02.002.

414 Briand, N., Prado, C., Mabilleau, G., Lasnier, F., Le Liepvre, X., Covington, J. D., Ravussin, E., Le Lay, S. and
415 Dugail, I. (2014) 'Caveolin-1 expression and cavin stability regulate caveolae dynamics in adipocyte lipid
416 store fluctuation', *Diabetes*, 63(12), pp. 4032–4044. doi: 10.2337/db13-1961.

417 Catalán, V., Gómez-Ambrosi, J., Rodríguez, A., Silva, C., Rotellar, F., Gil, M. J., Cienfuegos, J. A., Salvador,
418 J. and Frühbeck, G. (2008) 'Expression of caveolin-1 in human adipose tissue is upregulated in obesity
419 and obesity-associated type 2 diabetes mellitus and related to inflammation', *Clinical Endocrinology*,
420 68(2), pp. 213–219. doi: 10.1111/j.1365-2265.2007.03021.x.

421 Cham, B. E. and Knowles, B. R. (1976) 'A solvent system for delipidation of plasma or serum without
422 protein precipitation.', *Journal of lipid research*, 17, pp. 176–181.

423 Cheng, J. P. X. and Nichols, B. J. (2016) 'Caveolae : One Function or Many ?', *Trends in cell biology*.
424 Elsevier Ltd, 26(3), pp. 177–189.

425 Daumke, O., Lundmark, R., Vallis, Y., Martens, S., Butler, P. J. G. and McMahon, H. T. (2007)
426 'Architectural and mechanistic insights into an EHD ATPase involved in membrane remodelling.', *Nature*,
427 449(7164), pp. 923–7. doi: 10.1038/nature06173.

428 Ding, S. Y., Lee, M. J., Summer, R., Liu, L., Fried, S. K. and Pilch, P. F. (2014) 'Pleiotropic effects of cavin-1
429 deficiency on lipid metabolism', *Journal of Biological Chemistry*, 289(12), pp. 8473–8483. doi:
430 10.1074/jbc.M113.546242.

431 Drab, M., Verkade, P., Elger, M., Kasper, M., Lohn, M., Lauterbach, B., Menne, J., Lindschau, C., Mende,
432 F., Luft, F. C., Schedl, A., Haller, H. and Kurzchalia, T. V (2001) 'Loss of caveolae, vascular dysfunction, and
433 pulmonary defects in caveolin-1 gene-disrupted mice', *Science*, 293(5539), pp. 2449–2452. doi:
434 10.1126/science.1062688.

435 Dubikovskaya, E., Chudnovskiy, R., Karateev, G., Park, H. M. and Stahl, A. (2014) 'Measurement of long-
436 chain fatty acid uptake into adipocytes', *Methods Enzymol*, 538(1), pp. 107–134. doi:
437 10.3816/CLM.2009.n.003.Novel.

438 Eissing, L., Scherer, T., Tödter, K., Knippschild, U., Greve, J. W., Buurman, W. a, Pinnschmidt, H. O.,
439 Rensen, S. S. and Wolf, A. M. (2013) 'De novo lipogenesis in human fat and liver is linked to ChREBP- β
440 and metabolic health', *Nature Communications*, 4, pp. 1528–1539. doi: 10.1038/ncomms2537.De.

441 Eyre, N. S., Cleland, L. G., Tandon, N. N. and Mayrhofer, G. (2007) 'Importance of the carboxyl terminus
442 of FAT/CD36 for plasma membrane localization and function in long-chain fatty acid uptake', *Journal of*
443 *Lipid Research*, 48(3), pp. 528–542. doi: 10.1194/jlr.M600255-JLR200.

Grayson, T. H., Chadha, P. S., Bertrand, P. P., Chen, H., Morris, M. J., Senadheera, S., Murphy, T. V. and Sandow, S. L. (2013) 'Increased caveolae density and caveolin-1 expression accompany impaired NO-mediated vasorelaxation in diet-induced obesity', *Histochemistry and Cell Biology*, 139(2), pp. 309–321. doi: 10.1007/s00418-012-1032-2.

Guiu-Jurado, E., Auguet, T., Berlanga, A., Aragonès, G., Aguilar, C., Sabench, F., Armengol, S., Porras, J. A., Martí, A., Jorba, R., Hernández, M., del Castillo, D. and Richart, C. (2015) 'Downregulation of de novo fatty acid synthesis in subcutaneous adipose tissue of moderately obesewomen', *International Journal of Molecular Sciences*, 16(12), pp. 29911–29922. doi: 10.3390/ijms161226206.

Hansen, C. G., Howard, G. and Nichols, B. J. (2011) 'Pacsin 2 is recruited to caveolae and functions in caveolar biogenesis.', *Journal of cell science*, 124(Pt 16), pp. 2777–2785. doi: 10.1242/jcs.084319.

Hansen, C. G., Shvets, E., Howard, G., Riento, K. and Nichols, B. J. (2013) 'Deletion of cavin genes reveals tissue-specific mechanisms for morphogenesis of endothelial caveolae', *Nature Communications*. Nature Publishing Group, 4(May), pp. 1813–1831. doi: 10.1038/ncomms2808.

Hayer, A., Stoeber, M., Ritz, D., Engel, S., Meyer, H. H. and Helenius, A. (2010) 'Caveolin-1 is ubiquitinated and targeted to intralumenal vesicles in endolysosomes for degradation', *Journal of Cell Biology*, 191(3), pp. 615–629. doi: 10.1083/jcb.201003086.

Hill, M. M., Bastiani, M., Luetterforst, R., Kirkham, M., Kirkham, A., Nixon, S. J., Walser, P., Abankwa, D., Oorschot, V. M. J., Martin, S., Hancock, J. F. and Parton, R. G. (2008) 'PTRF-Cavin, a Conserved Cytoplasmic Protein Required for Caveola Formation and Function', *Cell*, 132(1), pp. 113–124. doi: 10.1016/j.cell.2007.11.042.

Hoernke, M., Mohan, J., Larsson, E., Blomberg, J., Kahra, D., Westenhoff, S., Schwieger, C. and Lundmark, R. (2017) 'EHD2 restrains dynamics of caveolae by an ATP-dependent, membrane-bound, open conformation.', *Proceedings of the National Academy of Sciences of the United States of America*, 114(22), pp. E4360–E4369. doi: 10.1073/pnas.1614066114.

Hsieh, F. L., Turner, L., Bolla, J. R., Robinson, C. V., Lavstsen, T. and Higgins, M. K. (2016) 'The structural basis for CD36 binding by the malaria parasite', *Nature Communications*. Nature Publishing Group, 7(May), pp. 1–11. doi: 10.1038/ncomms12837.

Ju, H., Zou, R., Venema, V. J. and Venema, R. C. (1997) 'Direct Interaction of Endothelial Nitric-oxide Synthase and Caveolin-1 Inhibits Synthase Activity', *The Journal of biological chemistry*, 272(30), pp. 18522–18525.

Kärgel, E., Menzel, R., Honeck, H., Vogel, F., Böhmer, a and Schunck, W. H. (1996) 'Candida maltosa NADPH-cytochrome P450 reductase: cloning of a full-length cDNA, heterologous expression in Saccharomyces cerevisiae and function of the N-terminal region for membrane anchoring and proliferation of the endoplasmic reticulum.', *Yeast (Chichester, England)*, 12(4), pp. 333–348. doi: 10.1002/(SICI)1097-0061(19960330)12:4<333::AID-YEA915>3.0.CO;2-C.

Kleinert, M., Clemmensen, C., Hofmann, S. M., Moore, M. C., Renner, S., Woods, S. C., Huypens, P., Beckers, J., De Angelis, M. H., Schürmann, A., Bakhti, M., Klingenspor, M., Heiman, M., Cherrington, A. D., Ristow, M., Lickert, H., Wolf, E., Havel, P. J., Müller, T. D. and Tschöp, M. H. (2018) 'Animal models of obesity and diabetes mellitus', *Nature Reviews Endocrinology*. Nature Publishing Group, 14(3), pp. 140–162. doi: 10.1038/nrendo.2017.161.

Kluth, O., Matzke, D., Kamitz, A., Jähnert, M., Vogel, H., Scherneck, S., Schulze, M., Staiger, H., Machicao, F., Häring, H.-U., Joost, H.-G. and Schürmann, A. (2015) 'Identification of Four Mouse Diabetes Candidate Genes Altering β-Cell Proliferation', *PLOS Genetics*. Edited by G. S. Barsh, 11(9), p. e1005506. doi:

487 10.1371/journal.pgen.1005506.

488 Kovtun, O., Tillu, V. A., Ariotti, N., Parton, R. G. and Collins, B. M. (2015) 'Cavin family proteins and the
489 assembly of caveolae', *Journal of cell science*, 128(7), pp. 1269–1278. doi: 10.1242/jcs.167866.

490 Kuerschner, L., Moessinger, C. and Thiele, C. (2008) 'Imaging of lipid biosynthesis: How a neutral lipid
491 enters lipid droplets', *Traffic*, 9(3), pp. 338–352. doi: 10.1111/j.1600-0854.2007.00689.x.

492 Le, P. U. (2003) 'Distinct caveolae-mediated endocytic pathways target the Golgi apparatus and the
493 endoplasmic reticulum', *Journal of Cell Science*, 116(6), pp. 1059–1071. doi: 10.1242/jcs.00327.

494 Le, P. U., Guay, G., Altschuler, Y. and Nabi, I. R. (2002) 'Caveolin-1 is a negative regulator of caveolae-
495 mediated endocytosis to the endoplasmic reticulum', *Journal of Biological Chemistry*, 277(5), pp. 3371–
496 3379. doi: 10.1074/jbc.M111240200.

497 Li, Z., Schulze, R. J., Weller, S. G., Krueger, E. W., Schott, M. B., Zhang, X., Casey, C. A., Liu, J., Stöckli, J.,
498 James, D. E. and McNiven, M. A. (2016) 'A novel Rab10-EHBP1-EHD2 complex essential for the
499 autophagic engulfment of lipid droplets', *Science Advances*, 2(12), pp. 1–16.

500 Liu, L., Brown, D., McKee, M., LeBrasseur, N. K., Yang, D., Albrecht, K. H., Ravid, K. and Pilch, P. F. (2008)
501 'Deletion of Cavin/PTRF Causes Global Loss of Caveolae, Dyslipidemia, and Glucose Intolerance', *Cell*
502 *Metabolism*, 8(4), pp. 310–317. doi: 10.1016/j.cmet.2008.07.008.

503 Liu, L., Hansen, C. G., Honeyman, B. J., Nichols, B. J. and Pilch, P. F. (2014) 'Cavin-3 knockout mice show
504 that cavin-3 is not essential for caveolae formation, for maintenance of body composition, or for glucose
505 tolerance', *PLoS ONE*, 9(7), pp. 1–8. doi: 10.1371/journal.pone.0102935.

506 Liu, P., Jenkins, N. A., Copeland, N. G., Liu, P., Jenkins, N. A. and Copeland, N. G. (2003) 'A Highly Efficient
507 Recombineering-Based Method for Generating Conditional Knockout Mutations', *Genome Research*, 13,
508 pp. 476–484. doi: 10.1101/gr.749203.

509 Ludwig, A., Howard, G., Mendoza-Topaz, C., Deerinck, T., Mackey, M., Sandin, S., Ellisman, M. H. and
510 Nichols, B. J. (2013) 'Molecular Composition and Ultrastructure of the Caveolar Coat Complex', *PLoS*
511 *Biology*, 11(8). doi: 10.1371/journal.pbio.1001640.

512 Ludwig, A., Nichols, B. J. and Sandin, S. (2016) 'Architecture of the caveolar coat complex.', *Journal of cell*
513 *science*, pp. 3077–3083. doi: 10.1242/jcs.191262.

514 Martin, S., Fernandez-Rojo, M. A., Stanley, A. C., Bastiani, M., Okano, S., Nixon, S. J., Thomas, G., Stow, J.
515 L. and Parton, R. G. (2012) 'Caveolin-1 Deficiency Leads to Increased Susceptibility to Cell Death and
516 Fibrosis in White Adipose Tissue: Characterization of a Lipodystrophic Model', *PLoS ONE*, 7(9), pp. 1–9.
517 doi: 10.1371/journal.pone.0046242.

518 Mehlem, A., Hagberg, C. E., Muhl, L., Eriksson, U. and Falkevall, A. (2013) 'Imaging of neutral lipids by oil
519 red O for analyzing the metabolic status in health and disease', *Nature Protocols*, 8(6), pp. 1149–1154.
520 doi: 10.1038/nprot.2013.055.

521 Melo, A. A., Hegde, B. G., Shah, C., Larsson, E., Isas, J. M., Kunz, S., Lundmark, R., Langen, R. and Daumke,
522 O. (2017) 'Structural insights into the activation mechanism of dynamin-like EHD ATPases', *Proceedings*
523 *of the National Academy of Sciences*, 114(22), pp. 5629–5634. doi: 10.1073/pnas.1614075114.

524 Mohan, J., Moren, B., Larsson, E., Holst, M. R. and Lundmark, R. (2015) 'Cavin3 interacts with cavin1 and
525 caveolin1 to increase surface dynamics of caveolae', *Journal of Cell Science*, 128(5), pp. 979–991. doi:
526 10.1242/jcs.161463.

527 Morén, B., Shah, C., Howes, M. T., Schieber, N. L., McMahon, H. T., Parton, R. G., Daumke, O. and

528 Lundmark, R. (2012) 'EHD2 regulates caveolar dynamics via ATP-driven targeting and oligomerization.',
529 *Molecular biology of the cell*, 23(7), pp. 1316–29. doi: 10.1091/mbc.E11-09-0787.

530 NIH Accelerating Medicines Partnership (2014) *Type 2 Diabetes Knowledge Portal*,
531 *http://www.type2diabetesgenetics.org*.

532 Ostermeyer, A. G., Paci, J. M., Zeng, Y., Lublin, D. M., Munro, S. and Brown, D. A. (2001) 'Accumulation of
533 caveolin in the endoplasmic reticulum redirects the protein to lipid storage droplets', *Journal of Cell*
534 *Biology*, 152(5), pp. 1071–1078. doi: 10.1083/jcb.152.5.1071.

535 Pelkmans, L., Bürli, T., Zerial, M. and Helenius, A. (2004) 'Caveolin-stabilized membrane domains as
536 multifunctional transport and sorting devices in endocytic membrane traffic', *Cell*, 118(6), pp. 767–780.
537 doi: 10.1016/j.cell.2004.09.003.

538 Pohl, J., Ring, A., Ehehalt, R., Schulze-Bergkamen, H., Schad, A., Verkade, P. and Stremmel, W. (2004)
539 'Long-Chain Fatty Acid Uptake into Adipocytes Depends on Lipid Raft Function', *Biochemistry*, 43(14), pp.
540 4179–4187. doi: 10.1021/bi035743m.

541 Pol, A., Gross, S. P. and Parton, R. G. (2014) 'Biogenesis of the multifunctional lipid droplet: Lipids,
542 proteins, and sites', *Journal of Cell Biology*, 204(5), pp. 635–646. doi: 10.1083/jcb.201311051.

543 Razani, B., Combs, T. P., Wang, X. B., Frank, P. G., Park, D. S., Russell, R. G., Li, M., Tang, B., Jelicks, L. A.,
544 Scherer, P. E. and Lisanti, M. P. (2002) 'Caveolin-1-deficient mice are lean, resistant to diet-induced
545 obesity, and show hypertriglyceridemia with adipocyte abnormalities', *Journal of Biological Chemistry*,
546 277(10), pp. 8635–8647. doi: 10.1074/jbc.M110970200.

547 Ring, A., Le Lay, S., Pohl, J., Verkade, P. and Stremmel, W. (2006) 'Caveolin-1 is required for fatty acid
548 translocase (FAT/CD36) localization and function at the plasma membrane of mouse embryonic
549 fibroblasts', *Biochimica et Biophysica Acta - Molecular and Cell Biology of Lipids*. Elsevier B.V., 1761(4),
550 pp. 416–423. doi: 10.1016/j.bbalip.2006.03.016.

551 Robenek, M. J., Severs, N. J., Schlattmann, K., Plenz, G., Zimmer, K. P., Troyer, D. and Robenek, H. (2004)
552 'Lipids partition caveolin-1 from ER membranes into lipid droplets: updating the model of lipid droplet
553 biogenesis.', *The FASEB journal : official publication of the Federation of American Societies for*
554 *Experimental Biology*, 18(7), pp. 866–868. doi: 10.1096/fj.03-0782fje.

555 Rutkowski, J. M., Stern, J. H. and Scherer, P. E. (2015) 'The cell biology of fat expansion', *Journal of Cell*
556 *Biology*, 208(5), pp. 501–512. doi: 10.1083/jcb.201409063.

557 Schlegel, A., Arvan, P. and Lisanti, M. P. (2001) 'Caveolin-1 binding to endoplasmic reticulum membranes
558 and entry into the regulated secretory pathway are regulated by serine phosphorylation. Protein sorting
559 at the level of the endoplasmic reticulum', *Journal of Biological Chemistry*, 276(6), pp. 4398–4408. doi:
560 10.1074/jbc.M005448200.

561 Seemann, E., Sun, M., Krueger, S., Tröger, J., Hou, W., Haag, N., Schüler, S., Westermann, M., Huebner,
562 C. A., Romeike, B., Kessels, M. M. and Qualmann, B. (2017) 'Deciphering caveolar functions by syndapin
563 III KO-mediated impairment of caveolar invagination', *eLife*, 6, pp. 1–37. doi: 10.7554/eLife.29854.

564 Senju, Y., Itoh, Y., Takano, K., Hamada, S. and Suetsugu, S. (2011) 'Essential role of PACSIN2/syndapin-II
565 in caveolae membrane sculpting', *Journal of Cell Science*, 124(12), pp. 2032–2040. doi:
566 10.1242/jcs.086264.

567 Shah, C., Hegde, B. G., Morén, B., Behrmann, E., Mielke, T., Moenke, G., Spahn, C. M. T., Lundmark, R.,
568 Daumke, O. and Langen, R. (2014) 'Structural insights into membrane interaction and caveolar targeting
569 of dynamin-like EHD2', *Structure*, 22(3), pp. 409–420. doi: 10.1016/j.str.2013.12.015.

570 Shvets, E., Bitsikas, V., Howard, G., Hansen, C. G. and Nichols, B. J. (2015) 'Dynamic caveolae exclude
571 bulk membrane proteins and are required for sorting of excess glycosphingolipids.', *Nature*
572 *communications*. Nature Publishing Group, 6, pp. 6867–6883. doi: 10.1038/ncomms7867.

573 Sinha, B., Köster, D., Ruez, R., Gonnord, P., Bastiani, M., Abankwa, D., Stan, R. V., Butler-Browne, G.,
574 Vedie, B., Johannes, L., Morone, N., Parton, R. G., Raposo, G., Sens, P., Lamaze, C. and Nassoy, P. (2011)
575 'Cells respond to mechanical stress by rapid disassembly of caveolae', *Cell*, 144(3), pp. 402–413. doi:
576 10.1016/j.cell.2010.12.031.

577 Solinas, G., Borén, J. and Dulloo, A. G. (2015) 'De novo lipogenesis in metabolic homeostasis: More
578 friend than foe?', *Molecular Metabolism*. Elsevier GmbH, 4(5), pp. 367–377. doi:
579 10.1016/j.molmet.2015.03.004.

580 Sonne, S. B., Yadav, R., Yin, G., Dalgaard, M. D., Myrmel, L. S., Gupta, R., Wang, J., Madsen, L., Kajimura,
581 S. and Kristiansen, K. (2017) 'Obesity is associated with depot-specific alterations in adipocyte DNA
582 methylation and gene expression', *Adipocyte*. Taylor & Francis, (May), pp. 1–10. doi:
583 10.1080/21623945.2017.1320002.

584 Sotgia, F., Razani, B., Bonuccelli, G., Schubert, W., Battista, M., Lee, H., Capozza, F., Schubert, A. L.,
585 Minetti, C., Buckley, J. T. and Lisanti, M. P. (2002) 'Intracellular retention of glycosylphosphatidyl
586 inositol-linked proteins in caveolin-deficient cells.', *Molecular and cellular biology*, 22(11), pp. 3905–
587 3926. doi: 10.1128/MCB.22.11.3905-3926.2002.

588 Stern, J. H., Rutkowski, J. M. and Scherer, P. E. (2016) 'Review Adiponectin , Leptin , and Fatty Acids in
589 the Maintenance of Metabolic Homeostasis through Adipose Tissue Crosstalk', *Cell Metabolism*. Elsevier
590 Inc., 23(5), pp. 770–784. doi: 10.1016/j.cmet.2016.04.011.

591 Stoeber, M., Schellenberger, P., Siebert, C. A., Leyrat, C., Helenius, A. and Grünewald, K. (2016) 'Model
592 for the architecture of caveolae based on a flexible, net-like assembly of Cavin1 and Caveolin discs.',
593 *Proceedings of the National Academy of Sciences of the United States of America*, p. 201616838. doi:
594 10.1073/pnas.1616838113.

595 Stoeber, M., Stoeck, I. K., Hänni, C., Bleck, C. K. E., Balistreri, G. and Helenius, A. (2012) 'Oligomers of the
596 ATPase EHD2 confine caveolae to the plasma membrane through association with actin', *The EMBO*
597 *Journal*, 31(10), pp. 2350–2364. doi: 10.1038/emboj.2012.98.

598 Torrino, S., Shen, W. W., Blouin, C. M., Mani, S. K., Lesegno, C. V. De and Bost, P. (2018) 'EHD2 is a
599 mechanotransducer connecting caveolae dynamics with gene transcription', pp. 1–14.

600 Uhlén, M., Fagerberg, L., Hallström, B. M., Lindskog, C., Oksvold, P., Mardinoglu, A., Sivertsson, Å.,
601 Kampf, C., Sjöstedt, E., Asplund, A., Olsson, I., Edlund, K., Lundberg, E., Navani, S., Szigyarto, C. A.,
602 Odeberg, J., Djureinovic, D., Takanen, J. O., Hober, S., Alm, T., Edqvist, P., Berling, H., Tegel, H., Mulder,
603 J., Rockberg, J., Nilsson, P., Schwenk, J. M., Hamsten, M., Feilitzen, K. Von, Forsberg, M., Persson, L.,
604 Johansson, F., Zwahlen, M., Heijne, G. Von, Nielsen, J. and Pontén, F. (2015) 'Tissue-based map of the
605 human proteome', 347(6220). doi: 10.1126/science.1260419.

606 Wilfling, F., Haas, J. T., Walther, T. C. and Jr, R. V. F. (2014) 'Lipid droplet biogenesis', *Current Opinion in*
607 *Cell Biology*. Elsevier Ltd, 29(1), pp. 39–45. doi: 10.1016/j.ceb.2014.03.008.

608 Wilfling, F., Wang, H., Haas, J. T., Krahmer, N., Gould, T. J., Uchida, A., Cheng, J. X., Graham, M.,
609 Christiano, R., Fröhlich, F., Liu, X., Buhman, K. K., Coleman, R. A., Bewersdorf, J., Farese, R. V. and
610 Walther, T. C. (2013) 'Triacylglycerol synthesis enzymes mediate lipid droplet growth by relocalizing
611 from the ER to lipid droplets', *Developmental Cell*, 24(4), pp. 384–399. doi:
612 10.1016/j.devcel.2013.01.013.

Wilkinson, D. D. (1993) ‘In situ Hybridization. A Practical Approach.’, *Genetical Research*. Cambridge University Press, 61(03), p. 234. doi: 10.1017/S0016672300031402.

617 **Figures**

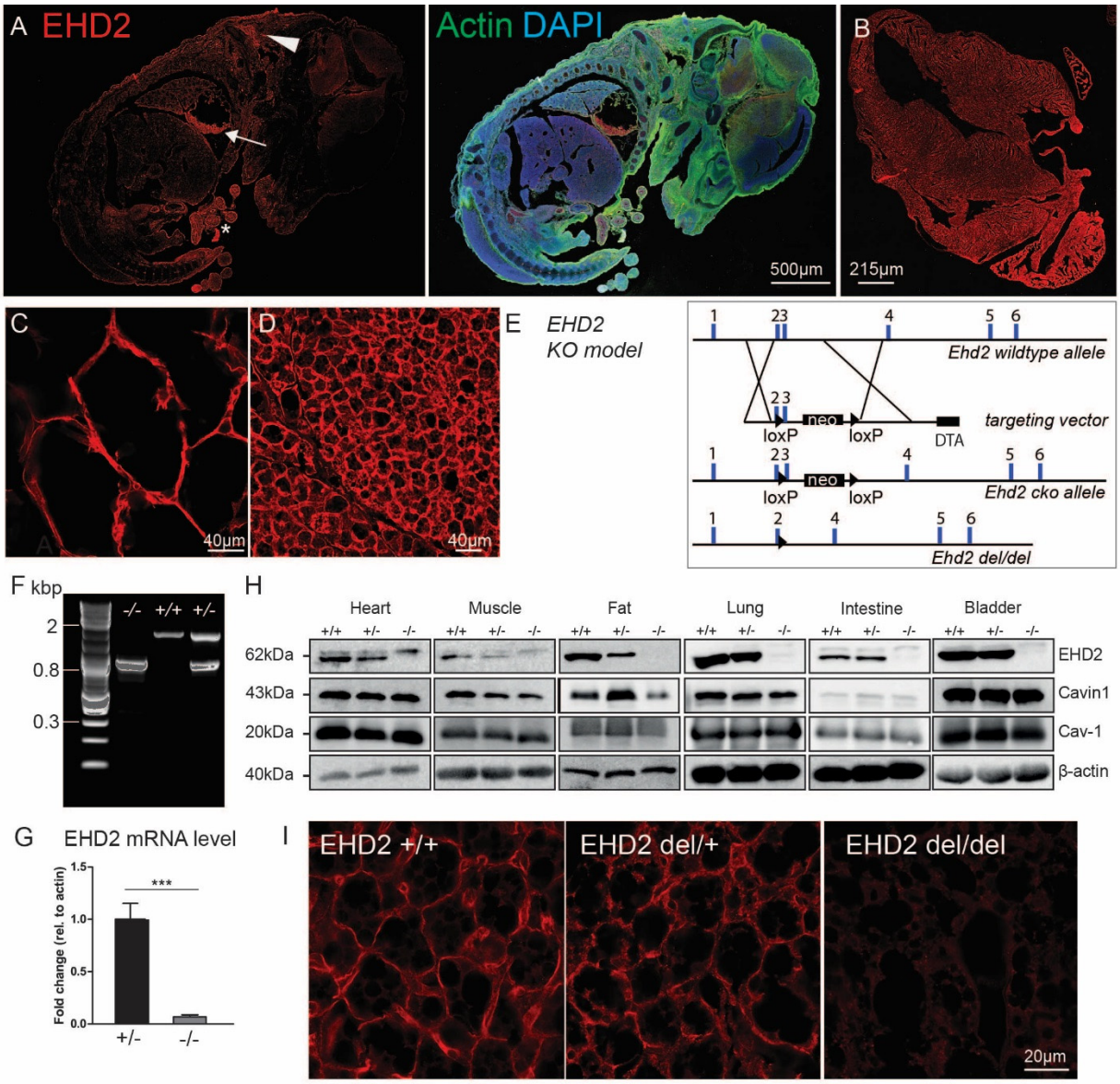

618

619 **Fig.1 EHD2 is strongly expressed in caveolae containing tissue**
620 **A** Cryostat section of a C57BL6/N E15 mouse embryo stained against EHD2 (red), actin (green) and the
621 nucleus (Blue, DAPI). White arrowhead indicates BAT, arrow indicates heart, star illustrates umbilical cord.
622 **B-D** Cryostat sections obtained from adult C57BL6/N heart (E), white (F) and brown (G) adipose tissue
623 were stained against EHD2 with an EHD2-specific antibody.
624 **E** Generation of the EHD2 KO mouse model. A targeting vector containing a pGK-Neomycin (neo) cassette
625 and loxP sites flanking exon 3 was placed in the EHD2 wt allele. EHD2 del/del mice were obtained by
626 breeding with Cre-deleter mouse strain (DTA - diphtheria toxin A).
627 **F** Genotyping of EHD2 delta E3 offspring (wildtype – band size 1,700 bp; EHD2 KO – band size 830 bp).
628 **G** EHD2 mRNA level in EHD2 del/+ and EHD2 del/del mice (mRNA from BAT, n = 5, bar column bar graph
629 represents mean + SE, Mann Withney U test, *** $P < 0.0001$).
630 **H** Western Blot analysis of different tissues in EHD2+/+, +/- and -/- mice against EHD2, Cav1 and Cavin1.
631 **I** EHD2 immuno-staining in BAT cryostat sections from EHD2 +/+, del/+ and del/del mice, see also Fig. S1.

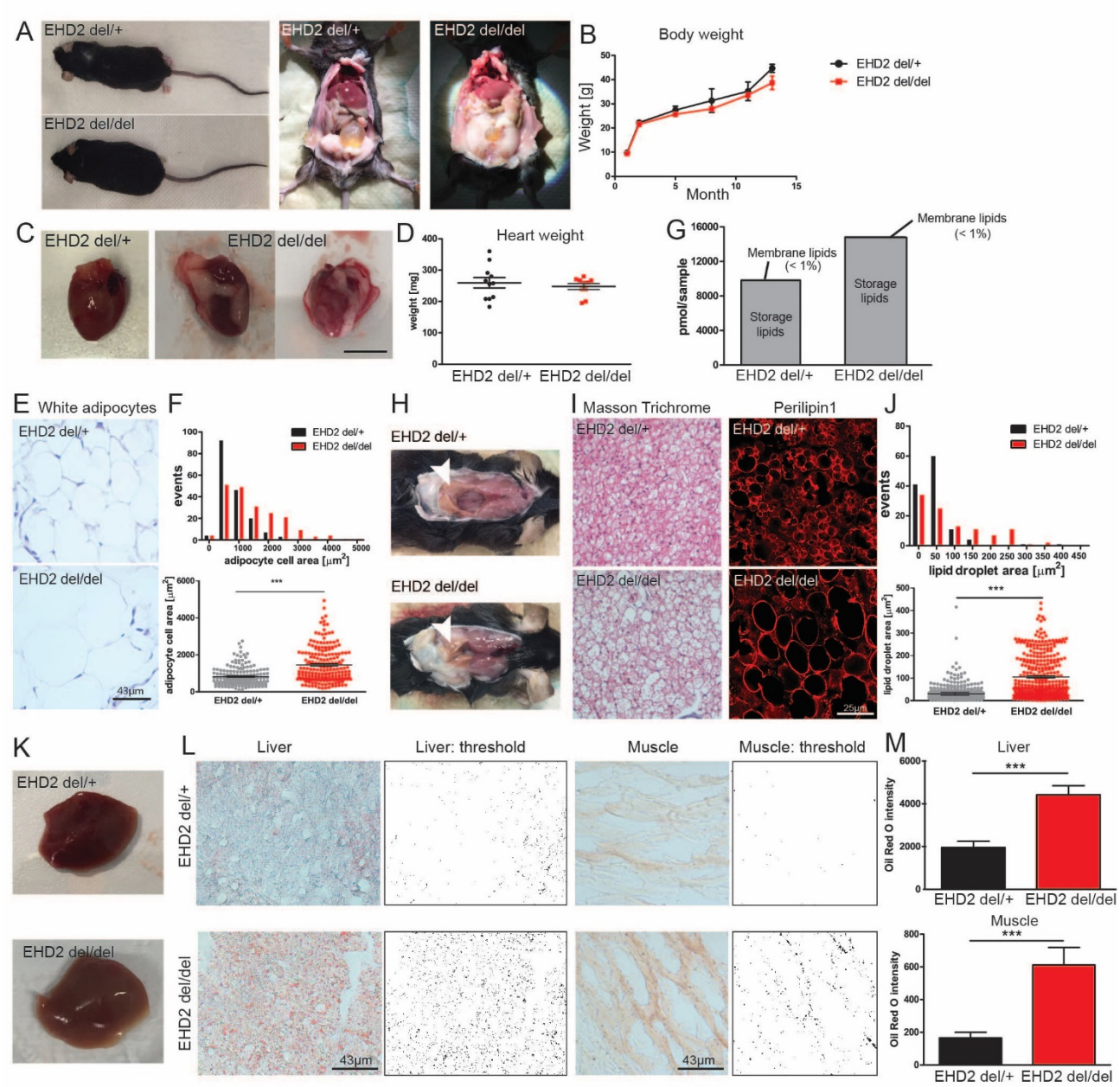

Fig. 2: Increased fat accumulation in EHD2 del/del mice

A-B EHD2 del/+ and EHD2 del/del mice during preparation (A). The body weight was monitored over 12 months (B, n = 7, line graph represents mean +/- SE).

C-D Illustration of EHD2 del/+ and del/del hearts (C, scale bar 1 cm) and its weight (D, n = 10).

E-F Masson Trichrome staining of WAT paraffin sections of EHD2 del/+ and EHD2 del/del. Detailed analysis of the adipocytes cell size (F, n(del/+) = 172/3, n(del/del) = 199/3).

G Lipid composition analysis of 15 µg WAT obtained from EHD2 del/+ or EHD2 del/del mice.

H EHD2 del/del mice showed decreased BAT in the neck region. Instead, WAT was integrated into the BAT depots.

I-J Masson Trichrome staining of EHD2 del/del BAT paraffin sections and BAT cryostat sections stained against the LD coat protein Perilipin1. LD size was measured in BAT cryostat sections (J, n(del/+) = 118/3, n(del/del) = 104/3).

645 **K-M** Representative image of liver obtained from EHD2 del/+ or del/del mice (K). Oil Red O staining of liver
646 and muscle tissue (L, M, n(liver) = 30/3, n(muscle) = 26/3).
647 Box plots indicate each replicate with mean +/- SE, column bar graphs show mean + SE, normal distributed
648 groups were analyzed by t-test, not normally distributed values with Mann Withney U test, * $P<0.05$, ***
649 $P<0.0001$. For comparison to C57BL6/N, see also Fig. S2.

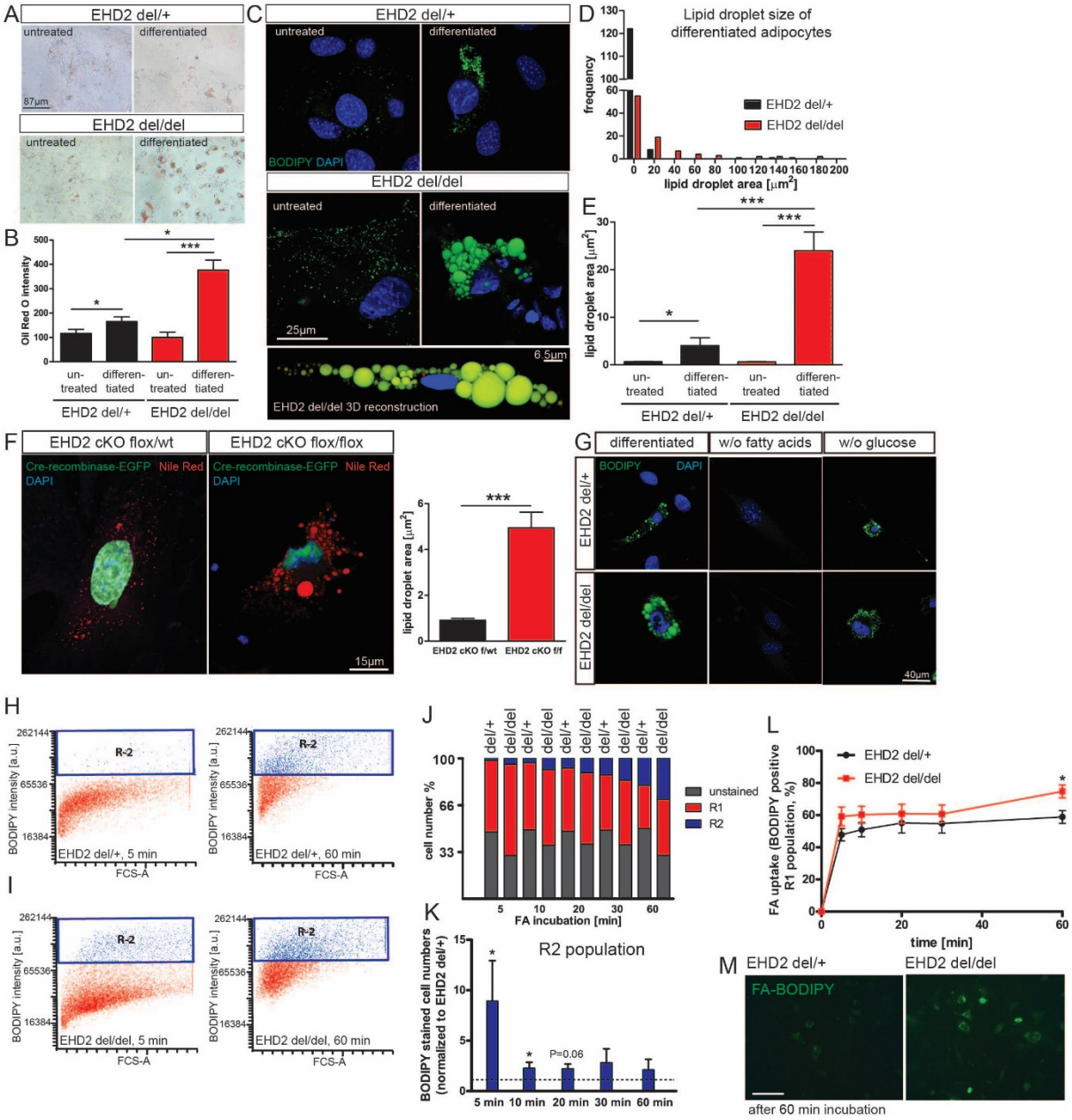

Fig. 3: EHD2 del/del adipocytes show faster fatty acid uptake

A-B Oil Red O staining of cultured untreated pre-adipocytes and differentiated adipocytes (untreated: n(del(+) = 41/4, n(del/del) = 36/4); differentiated: n(del/+) = 84/6, n(del/del) = 106/8).

C-E Analysis of LD size in EHD2 del/del and EHD2 del/+ adipocytes by staining with BODIPY (untreated: n(del(+) = 74/3, n(del/del) = 60/3); differentiated: n(del/+) = 132/3, n(del/del) = 95/3). 3D reconstruction of EHD2 del/del differentiated adipocyte. Green – LDs, blue – nucleus.

F Cultivated EHD2 cKO flox/wt or flox/flox adipocytes were transfected with Cre recombinase-EGFP to induce EHD2 deletion and differentiated for 5 days, lipid droplets were stained with Nile Red for analysing (n(flox/wt) = 74/2, n(flox/flox) = 82/2).

663
664 **G** Pre-adipocytes were treated with either differentiation medium containing delipidated FBS or without
665 glucose and BODIPY staining illustrating LDs.
666
667 **H-I** Fatty acid uptake assay in differentiated EHD2 del/+ and EHD2 del/del adipocytes. Dodecanoic acid-
668 BODIPY uptake was measured after 5, 10, 20, 30 or 60 min, and R1 population indicates positively stained
669 cells (illustrated in red in graphs H, I). R2 populations (blue) correspond to higher BODIPY staining intensity
670 in cells and represent adipocytes with increased amount of dodecanoic acid taken up (shown in blue in
671 graphs H, I).
672
673 **J-M** Overview of fatty acid uptake (percent cell numbers (J), normalization of EHD2 del/del R2 population
674 relative to EHD2 del/+ R2 (K), time scale (L); J-L, n(del/+) = 6/3 experiments, n(del/del) = 8/3 experiments).
675 Example images of differentiated adipocytes treated with dodecanoic acid for 60 min (M, scale bar 40
676 µm).
677 Column bar graphs and line graphs illustrate mean +/- SE, t-test or Mann Withney U test were used to
678 calculate significance, * $P<0.05$; *** $P<0.0001$. See also Fig. S3.
679

680

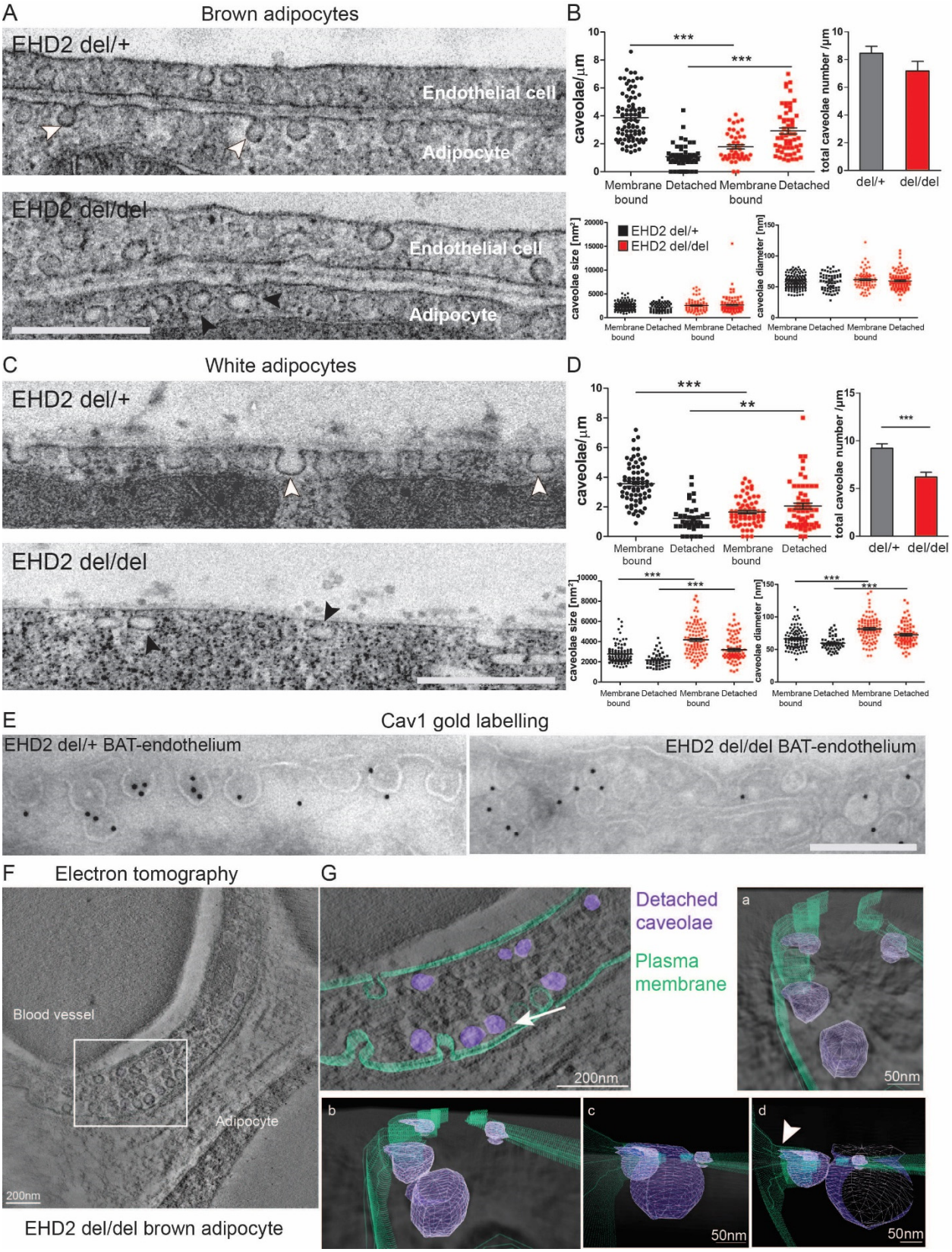
A
Brown adipocytes
EHD2 del/+
Endothelial cell
Adipocyte
EHD2 del/del
Endothelial cell
Adipocyte
B
caveolae/µm
Membrane bound
Detached
Membrane bound
Detached
total caveolae number /µm
del/+
del/del
EHD2 del/+
EHD2 del/del
caveolae size [nm²]
caveolae diameter [nm]
C
White adipocytes
EHD2 del/+
EHD2 del/del
D
caveolae/µm
total caveolae number /µm
caveolae size [nm²]
caveolae diameter [nm]
E
Cav1 gold labelling
EHD2 del/+ BAT-endothelium
EHD2 del/del BAT-endothelium
F
Electron tomography
Blood vessel
Adipocyte
200nm
EHD2 del/del brown adipocyte
G
Detached caveolae
Plasma membrane
200nm
a
50nm
b
c
50nm
d
50nm

681

682 **Fig. 4: Loss of EHD2 resulted in detached caveolae *in vivo***

683 **A-B** Representative EM images of BAT from EHD2 del/+ and del/del mice and systematic analysis (caveolae
684 number: n(del/+) = 140/3, n(del/del) = 100/3; caveolae size and diameter: n(del/+) = 201/3, n(del/del) =
685 171/3). Scale bar 500 nm.

686 **C-D** EM images of EHD2 del/+ and del/del WAT (caveolae number: n(del/+) = 108/3, n(del/del) = 124/3;
687 caveolae size and diameter: n(del/+) = 151/3, n(del/del) = 185/3). Scale bar 500 nm.

688 **E** Representative image for EM gold immunolabeling against Cav1. Control labeling did not reveal specific
689 staining. Scale bar 200 nm.

690 **F-G** Electron tomogram of a 150 nm EHD2 del/del BAT section (F). The 3D model contains the plasma
691 membrane (G, green) and the detached caveolae (violet). Detachment of caveolae was observed by
692 changing the viewing angle (white arrow indicates the direction). Closer inspection of cell membrane and
693 caveolae clearly showed displacement of caveolae from the membrane. The 3D model also revealed
694 attachment of caveolae to the membrane (arrow head).

695 Graphs illustrate each replicate with mean +/- SE, t-test or Mann Withney U test were used to calculate
696 significance, ** P<0.001; *** P<0.0001. See also Movie S1.

697

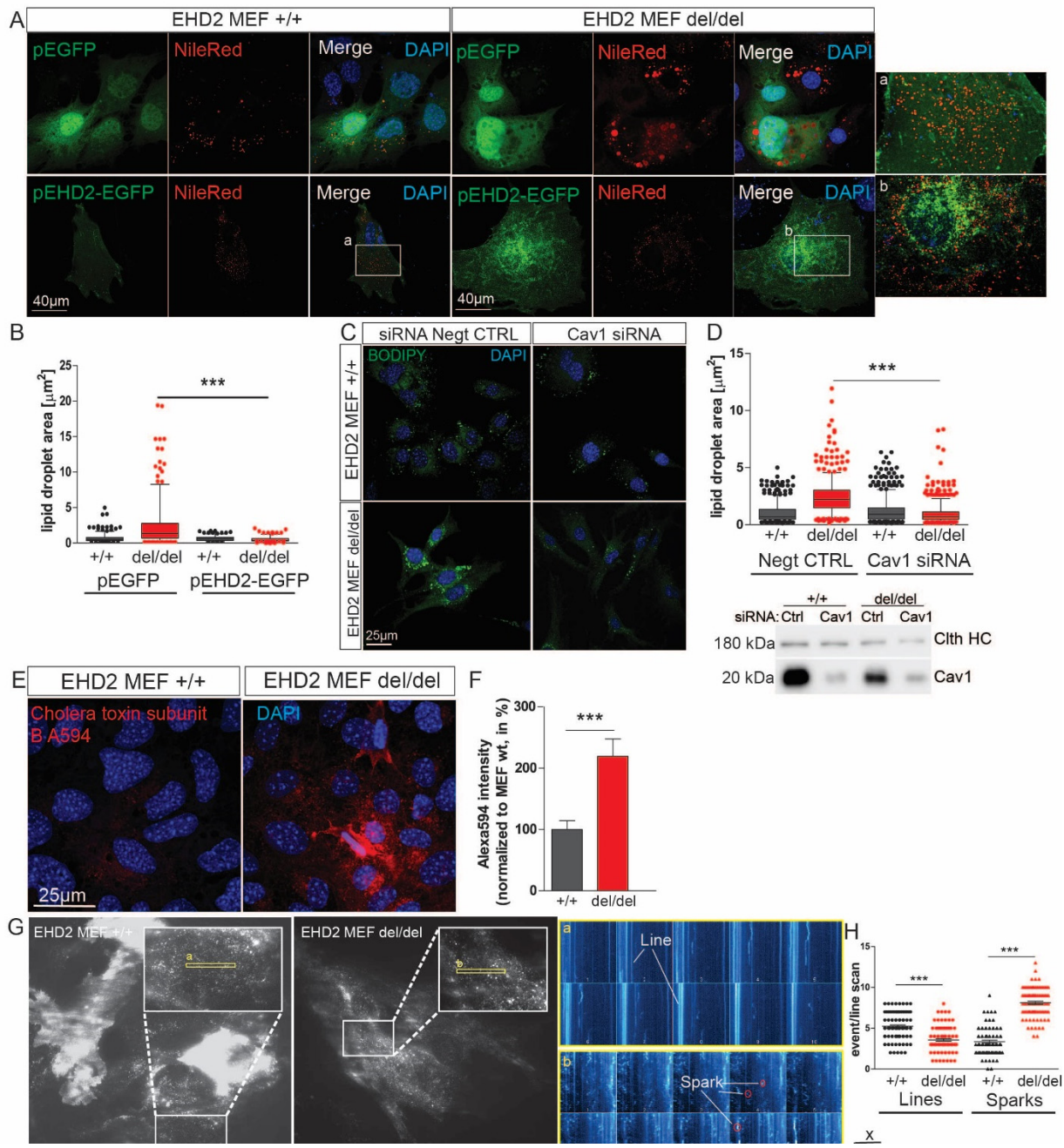

Fig. 5: Enhanced caveolar mobility in cells lacking EHD2

A-B EHD2 +/+ and del/del MEFS were transfected with either pEGFP or pEHD2-EGFP, incubated for 48 h and afterwards treated for 6 h with oleic acid and Nile Red staining was performed to determine LDs (pEGFP: n(+/+) = 309/3, n(del/del) = 310/3; pEHD2-EGFP: n(+/+) = 218/4, n(del/del) = 184/4).

C-D EHD2 del/del MEFs were treated with Cav1 siRNA and lipid droplets were stained with BODIPY (negative control: n(+/+) = 504/3, n(del/del) = 530/3; Cav1 siRNA: n(+/+) = 521/3, n(del/del) = 558/3); Clth HC - clathrin heavy chain.

E-F EHD2 MEFs were treated with Cholera toxin subunit B Alexa594 uptake in EHD2 +/+ and del/del MEFs after 30 min (F, n(+/+) = 40/5, n(del/del) = 40/6).

G-H TIRF live-imaging of EHD2 +/+ and del/del MEFs expressing pCav1-EGFP**.** Line scan analysis of the recorded Cav1 intensities revealed for fixed, non-moving caveolae lines and for fast moving caveolae

710 single sparks (as illustrated in a and b, n(+/+) = 90/3; n(del/del) = 92/3; each replicate is represented with
711 mean +/- SE).
712 Box plots indicate maximal to minimum value with median, column bar graphs show mean + SE, t-test or
713 Mann Withney U test were used to calculate significance, *** P<0.0001. See also Fig. S4 and Movie S2-4.

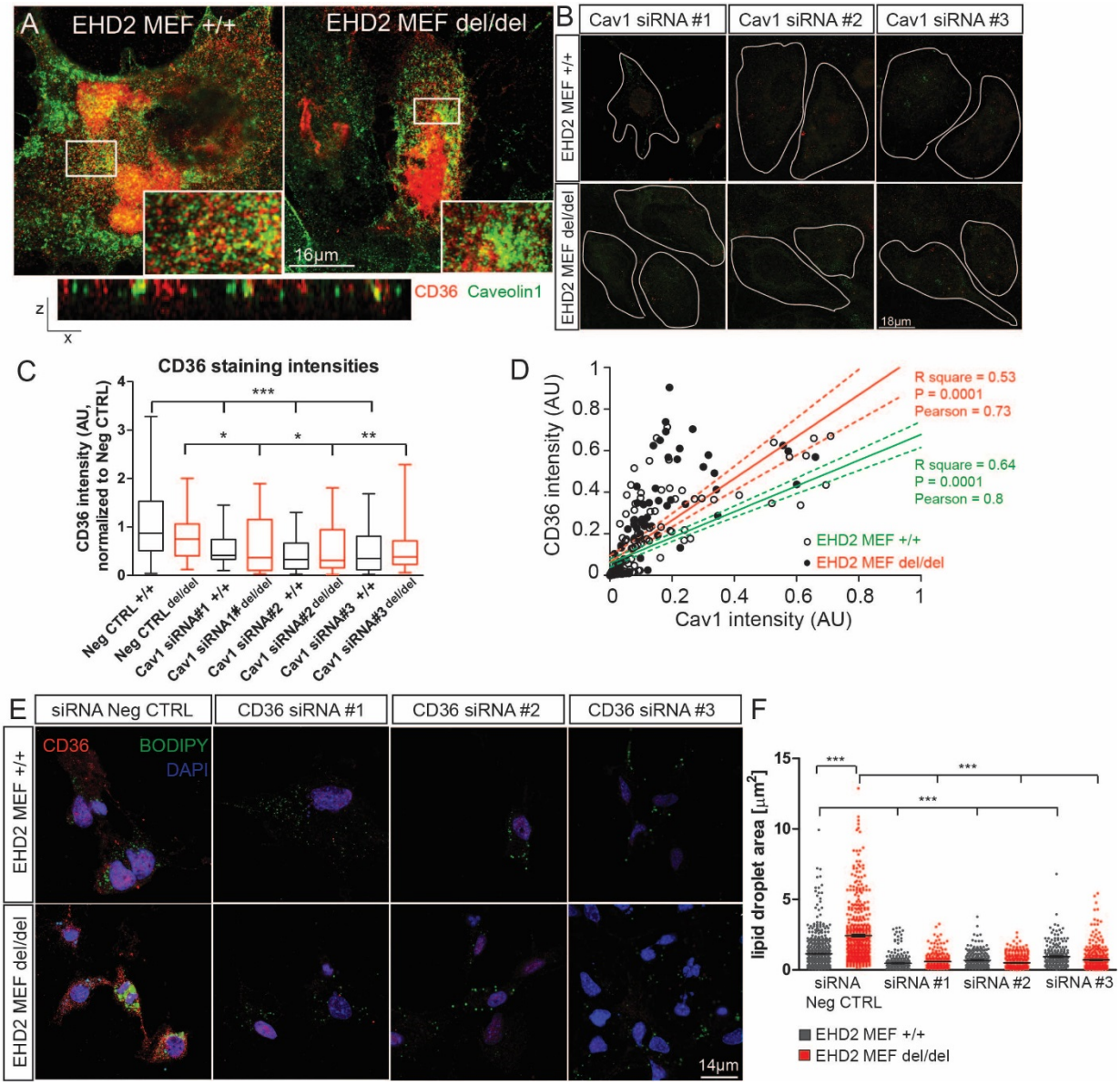

Fig. 6 Fatty acid translocase CD36 is involved in EHD2-mediated fatty acid uptake

A CD36 localization was investigated by antibody staining in EHD2 +/+ and del/del MEFs. Partial co-localization of CD36 and Cav1 was observed by confocal airyscan z-stack imaging.

B Example images for CD36 and Cav1 staining after Cav1 siRNA treatment in EHD2 +/+ and del/del MEFs (cells are indicated by white surrounding lines, compare to staining in A).

C Fluorescence intensity measurement of Cy3-Rabbit antibody after Rabbit-CD36 live staining in Cav1 siRNA treated MEFs (negative control: n(+/+) = 584/6, n(del/del) = 475/6; Cav1 siRNA#1: n(+/+) = 341/3, n(del/del) = 249/3; Cav1 siRNA#2: n(+/+) = 412/3, n(del/del) = 468/3; Cav1 siRNA#3: n(+/+) = 251/3, n(del/del) = 368/3; box plots indicate median with whiskers from maximal to minimum value, siRNA negative control was compared to Cav1 siRNA for statistical analysis).

D Correlation of Cav1 and CD36 staining intensities in EHD2 +/+ and del/del MEFs (n(+/+) = 150/4, n(del/del) = 120/4; Pearson correlation; graph shows each replicate and related linear regression including 95% confidence interval).

728 **E-F** LD size after CD36 siRNA knockdown in EHD2 +/+ and del/del MEFs (D, negative control: n(+/+) =
729 584/6, n(del/del) = 475/6; CD36 siRNA#1: n(+/+) = 341/3, n(del/del) = 249/3; CD36 siRNA#2: n(+/+) =
730 412/3, n(del/del) = 468/3; CD36 siRNA#3: n(+/+) = 251/3, n(del/del) = 368/3; graph illustrates each
731 replicate with mean +/- SE, 2-way ANOVA test were used to calculate significance between siRNA negative
732 CTRL and siRNA, t-test was used between +/+ and del/del data).
733 *P<0.05, **P<0.001, ***P<0.0001. See also Fig. S5.

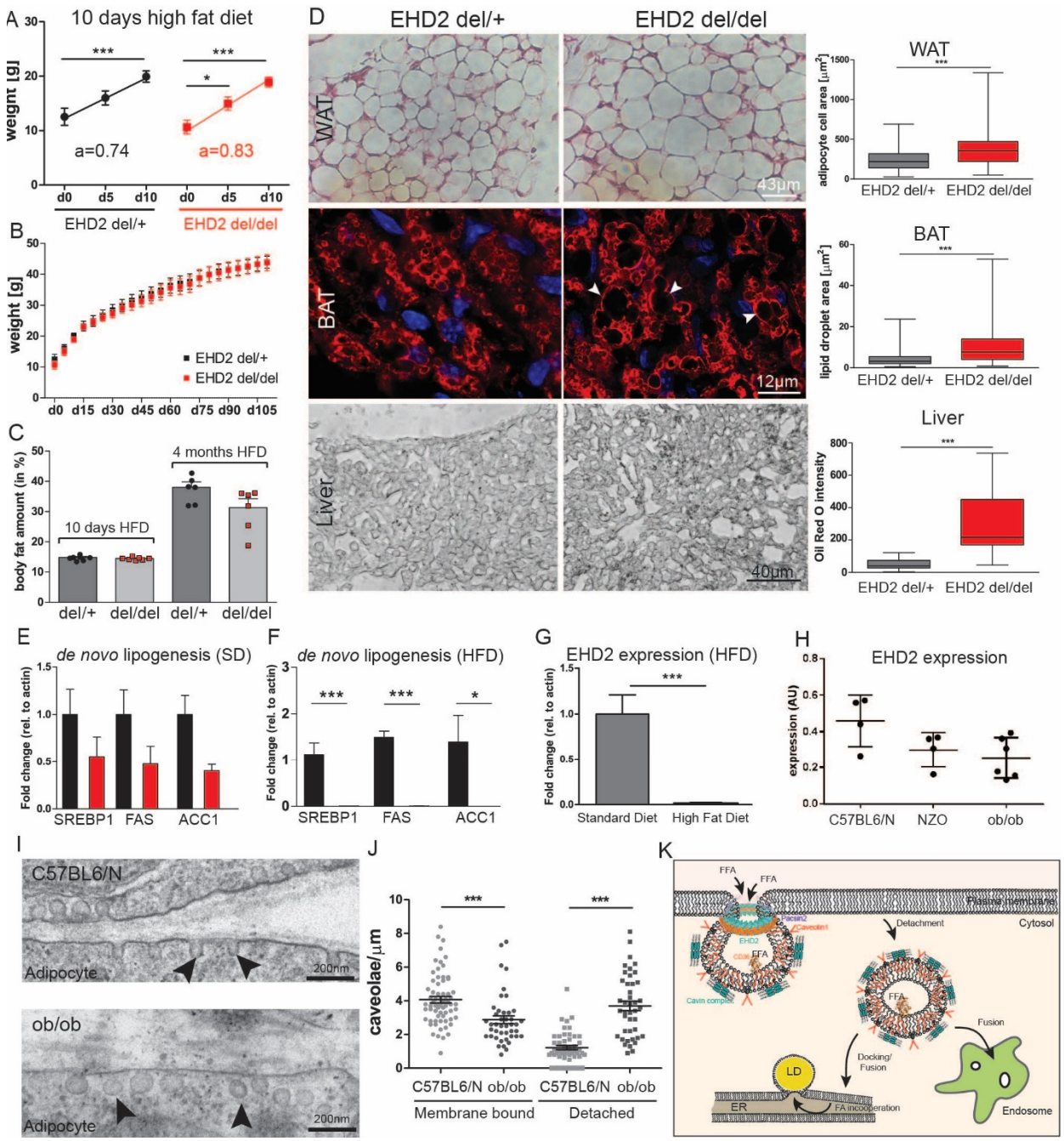

Fig. 7: Decreased EHD2 expression in diet induced obesity and genetic obesity mouse models

A-B EHD2 del/+ and EHD2 del/del mice were fed with a high fat diet (60% kcal fat) for 10 days (A) or 4 months (B) and body weight was measured every 5 days (A, n(day 0-10) = 12; B, n(day 15-110) = 6).

C Body composition analysis after 10 days or 4 months of high fat diet (n(10 days high fat diet) = 7; n(4 months of high fat diet) = 6).

D After 10 days high fat feeding, adipocyte cell sizes were analyzed in EHD2 del/+ and EHD2 del/del WAT paraffin sections (n(del/+) = 317/2; n(del/del) = 337/2). BAT cryostat sections were stained against Perilipin1 (red – Perilipin1, blue – DAPI; n(del/+) = 263/2; n(del/del) = 236/2). Oil Red O staining of liver

744 sections obtained from EHD2 del/+ and EHD2 del/del mice fed for 10 days with high fat diet (n(del/+) =
745 28/2; n(del/del) = 29/2).
746 **E-F** Expression levels of genes involved in *de novo* lipogenesis in EHD2 del/del and del/+ WAT following
747 standard diet (SD, E) or high fat diet (HFD, F; n(SD) = 8-12/4; HFD, n(del/+) = 8/3, n(del/del) = 6/3).
748 **G** EHD2 expression in white adipocytes of EHD2 del/+ mice fed with high fat diet (HFD) compared to EHD2
749 del/+ mice under standard diet (n = 5).
750 **H** EHD2 expression level was analyzed in fat tissue of ob/ob or NZO mouse models compared to C57BL6/N
751 mice (n = 5, graph illustrates mean +/- SE).
752 **I-J** Investigation of caveolae by EM imaging (n(ob/ob mice) = 85/2; n(C57BL6/N) = 117/2; graph illustrates
753 mean +/- SE).
754 **K** The model illustrates the EHD2-caveolae dependent fatty acid uptake. CD36 localizes within caveolae,
755 consequently, CD36 can bind and transfer free fatty acids (FFA) through the plasma membrane (PDB:
756 5LGD, (Hsieh *et al.*, 2016)). After loss of EHD2, the enhanced mobility and detachment of caveolae results
757 in an increased fatty acid uptake either via direct fusion or docking to the ER or via the endosomal pathway
758 (FFA - free fatty acid, ER – endoplasmic reticulum, LD – lipid droplet).
759 Box plots indicate median with whiskers from maximal to minimum value, column bar and line graphs
760 show mean +/- SE, normal distributed groups were analyzed by t-test, not normal distributed values with
761 Mann Withney U test, * $P<0.05$, *** $P<0.0001$. See also Fig. S5-6.
762

763 **Material and Methods**

764 **EHD2 delta E3 mouse strain generation.** The EHD2 targeting construct was generated by insertion of two
765 lox P sequences flanking exon 3 of EHD2 genomic DNA by homologous recombination in *E.coli* as
766 previously described (Liu *et al.*, 2003). A pGK Neomycin and a diphtheria toxin A (DTA) cassette was
767 included to enrich for correctly targeted ES cells. Electroporation of the linearized targeting vector in R1
768 ES cells was performed. For southern blot analysis, genomic DNA from G418-resistant ES clones was
769 digested with BamHI and EcoRV and probed with PCR fragments to confirm correct integration (BamHI-
770 Probe: Primer-FWD: 5- CACGCGGTCCAGCTGGCTTCA-3', Primer-REV: 5'- GTG GCT GAA GAG TCT ATG CAC
771 TTC GAG-3'; EcoRV-Probe: Primer-FWD: 5'- CAG GCC CCA CGC TTC AGG ATT TTA ACT G-3', Primer-REV:
772 5'- GCC TTG TTG AGT ACC ACG CGG ATC-3'). Correctly targeted ES clones were injected into C57Bl6
773 blastocyst. The offspring was genotyped by PCR. Mice carrying a loxP-flanked Exon 3 of EHD2 gene were
774 mated to Cre deleter mice to generate EHD2 mutant (del/del) mice. After backcrossing the EHD2 del/del
775 mice with C57BL6/N (Charles River, between 20-30 weeks, male) for 6 generations only male EHD2 del/del
776 or EHD2 del/+ (as control) mice were used and littermates were randomly assigned to experimental
777 groups. All animals were handled accordingly to governmental animal welfare guidelines and were housed
778 under standard conditions. If not otherwise indicated mice were sacrificed at an age of 20-30 weeks (for
779 cell culture preparation) or 40-50 weeks (organ dissection).

780 **Obesity Mouse Models.** Male NZO/HIBomDife (German Institute of Human Nutrition, Nuthetal,
781 Germany), C57BL/6J (Charles River Laboratories, Sulzfeld, Germany) and B6.V-Lepob/ob/JBomTac (B6-
782 ob/ob) mice (Charles River Laboratories, Calco, Italy) were housed under standard conditions
783 (conventional germ status, 22 °C with 12 hour /dark cycling). NZO and C57BL/6J mice were fed were fed
784 standard chow diet (Ssniff, Soest). Starting at 5 weeks of age B6-ob/ob received carbohydrate free diet
785 (Kluth *et al.*, 2015). Mice were sacrificed at an age of 20-22 weeks.

786 **High Fat Diet.** To investigate *in vivo* fat uptake the EHD2 delta E3 mice were fed with a high fat diet
787 (OpenSource Diets, D12492, 60% kcal) according to our animal application. In total, 16 EHD2 del/+ and 16
788 EHD2 del/del mice were investigated whereby only male, backcrossed animals were used (>F5 generation,
789 backcrossing with C57BL6/N). The high fat diet was immediately applied after weaning for maximal 16
790 weeks. The body weight was monitored every 5 days. 7 mice/genotype were fed for 10 days with high fat
791 diet and afterwards the body composition (BRUKER MiniSpec LF90II) was measured.

792 **Mouse embryonic fibroblast isolation and immortalization.** All animals were handled accordingly to
793 governmental animal welfare guidelines. MEFs were obtained from E14.5 EHD2 +/+ or del/del embryos.
794 Therefore female, pregnant EHD2 del/+ were sacrificed by cervical dislocation, the embryos were

795 dissected and removed from the yolk sac in sterile, cold PBS. For genotyping, a small piece of each mouse
796 embryo tail was harvested followed by complete dissection of the whole embryo. Afterwards, the embryo
797 pieces were treated with 0.25% trypsin/EDTA (Sigma) over night at 4 °C. After aspiration of the trypsin
798 solution, 10 ml culture medium (DMEM/10%FBS/5% penicillin/streptomycin) was added and tissue pieces
799 were break up by pipetting. The cell suspension was transferred in 75 cm^2 culture flask for cultivation at
800 37 °C and 5% CO_2. Immortalization of isolated primary MEFs was assured by frequently splitting. From
801 passage 15 an increased growth rate was observed suggesting immortalized MEFs. For all experiments
802 MEFs between passage 12 and 32 was used. For LD growth, MEFs were either treated with 10 µg/ml
803 insulin, 2.5 mM dexamethasone, 50 mM IBMX and 25 mM rosiglitazone diluted in culture medium
804 (differentiation medium) or 0.016 M oleic acid and 10 µg/ml insulin diluted in DMEM.
805 **Primary adipocyte cell culture.** Male EHD2 del/+ and EHD2 del/del mice or EHD2 cKO flox/wt or flox/flox
806 were sacrificed by cervical dislocation and gonadal WAT was removed. Adipocytes and stromal vascular
807 fraction (SVF) were isolated after washing the tissue in sterile PBS and digestion by collagenase type II
808 (Sigma C6885). Mature adipocytes floating in the upper phase were transferred in a new flask and diluted
809 with culture medium (DMEM/10%FBS/5% penicillin/streptomycin), SVF was obtained after 5 min
810 centrifugation at 1,000 rpm. After complete tissue break up the adipocyte cell suspension was passed
811 through a 270 µm cell strainer and the cells were plated in 75 cm^2 culture flask at 37 °C and 5% CO_2
812 whereby pre-adipocytes adhere to the flask and mature adipocytes float in the medium. SVF suspension
813 was cleaned by passing through 70 µm cell strainer. The following day the culture medium was exchanged
814 to remove dead or non-adherent cells. After 5 days, both pre-adipocytes and SVF were split by 0.25%
815 trypsin/EDTA solution and merged for further cultivation. Differentiation to mature adipocytes was
816 induced by 10 µg/ml insulin, 2.5 mM dexamethasone, 50 mM IBMX and 25 mM rosiglitazone diluted in
817 culture medium. If not otherwise mentioned the primary pre-adipocytes were incubated for 5 days with
818 differentiation medium and medium was changed after 2 days. Delipidation of FBS was carried out as
819 described by (Cham and Knowles, 1976). EHD2 cKO adipocytes were transfected with Cre recombinase-
820 EGFP by using adeno-associated virus particles 8 (AAV8) produced from pAAV.CMV.HI.eGFP-
821 Cre.WPRE.SV40 (addgene, #105545). The adipocyte cell culture was transfected and differentiated for 5
822 days.
823 **Oil Red O staining.** LDs in tissue sections or cultivated adipocytes and MEFs were stained with Oil Red O
824 as published by (Mehlem *et al.*, 2013). Briefly, freshly dissected liver of muscle pieces were frozen in liquid
825 nitrogen, embedded in TissueTek and 10 µm cryostat sections (Leica) were prepared. After fixation with
826 4% para-formaldehyde (PFA, Merck) freshly prepared Oil Red O staining solution was applied for 10 min.

827 The sections were washed with PBS and embedded in ImmoMount (Invitrogen). Cultivated cells were
828 fixed, treated with 60% isopropanol (Merck) for 2 min and then incubated with Oil Red O staining solution
829 for 5 min. After washing with water until complete removal of Oil Red O the stained cells or sections were
830 analyzed by Zeiss Axiovert microscope (20x Zeiss objective). Staining intensity was measured with ImageJ.
831 **Histology.** EHD2 del/+ and EHD2 del/del mice were anesthetized with 2% ketamine/10%rompun, perfused
832 first by 30 ml PBS and next by 50 ml 4% PFA and tissues were dissected. After 24 h of fixation in 4% PFA,
833 tissues were dehydrated in 3 steps (each 24h) from 70-100% EtOH and afterwards incubated in xylol
834 (Merck) for 48 h. Next, the tissues were embedding in liquid paraffin at ca. 65°C and cooled down on ice.
835 4 µm paraffin sections were obtained, de-paraffinized and hydrated and Masson Trichrome staining (Kit,
836 Sigma) was applied. Briefly, sections were stained with Bouin solution for 15 min at 60°C, followed by
837 Haematoxylin Gill No. 2 staining for 5 min and incubation in Biebrich-Scarlet-Acid Fuchsin for 5 min. Next,
838 the tissue sections were treated with Phosphotungstic/Phosphomolybdic Acid Solution and Aniline Blue
839 solution both for 5 min, and acetic acid treatment (1%) for 2 min. After extensive washing the sections
840 were dehydrated, incubated in xylol and embedded with Roti Histo Kit (Carl Roth). Images were obtained
841 at Zeiss Axiovert100 microscope.
842 **Immunohistostaining of cryostat sections.** Perfused and fixated EHD2 del/+ and EHD2 del/del mice (as
843 described before) were dissected and the investigated tissue pieces were further fixed for 1-4 h in 4% PFA,
844 transferred to 15% sucrose (in PBS, Merck) for 4 h and finally incubated overnight in 30% sucrose. After
845 embedding in TissueTek, the tissue is frozen at -80 °C. 5-15 µm sections were obtained in a cryostat at -
846 20 - -30 °C and stored at -20 °C. For immunostainings, the cryostat sections were incubated with blocking
847 buffer (1% donkey serum/1% TritonX100/PBS) for 1 h at room temperature, and treated overnight at 4°C
848 with the first antibody diluted in blocking buffer. After washing with PBS/1%Tween, the secondary
849 antibody was applied for 2 h at room temperature. After completion of the staining, the sections were
850 washed carefully and embedded in ImmoMount. The stained sections were analyzed with Zeiss LSM700
851 microscope provided with Zeiss objectives 5, 10, 20, 40 and 63x. The obtained images were further
852 investigated by ZEN software and ImageJ/Fij.
853 **Immunocytostaining and LD staining of cultivated cells.** Adipocytes or MEFs were seeded on fibronectin
854 (Sigma) coated glass dishes (12 mm diameter, Thermo Fisher) in cell concentration ranging from 20.000-
855 40.000 cells/well depending on treatment and experiment. Before the staining, cells were washed with
856 PBS, treated with 4% PFA for 10 min and blocking buffer (1%donkey serum/1% TritonX100/PBS) was
857 applied for 20 min. The first antibody was diluted in blocking buffer and the cells were incubated with 200
858 µl antibody solution for 1 h. After washing with PBS the secondary antibody and DAPI (1:1000, Sigma) was

859 applied for 1 h. For LD staining, BODIPY (Invitrogen) or Nile Red (Sigma) was diluted to 1:500 in cold PBS
860 and after washing and fixation of the cells, the BODIPY or Nile Red staining solution and DAPI (1:1000) was
861 applied for 30 min. The stained cells were washed and the glass dishes were placed on conventional
862 microscope slides and embedded in ImmoMount. The antibody staining was investigated by Zeiss LSM700
863 or Zeiss LSM880 microscope and images were analyzed in detail with ImageJ/Fij.
864 **Transfection and siRNA knockdown.** Cultivated MEFs were transfected with the following plasmids
865 pEHD2-EGFP, pCav1-EGFP or pEGFP by lipofectamine 3000 accordingly to the manufacture's protocol.
866 Transfected cells were incubated for 48 h and afterwards the treated cells were analyzed by confocal
867 microscopy or TIRF. siRNA knockdown of CD36 or Cav1 was performed in freshly split MEFs by
868 electroporation with the GenePulser XCell (Biorad). Briefly, MEFs were split as described before and the
869 obtained cell pellet was resuspended in OptiMEM (Gibco). After cell counting, the MEF cell suspension
870 was diluted to $1.5x10^6$ cells/ml and 300 µl were transferred into electroporation cuvettes (2 mm, Biorad).
871 CD36 or Cav1 stealth siRNA and siRNA negative control (medium GC content) was added to a final
872 concentration of 200 nM. After carful mixing, the cuvettes were placed into the electroporation device
873 and the pulse (160 µOHM, 500 µF, ∞ resistance) was applied. The electroporated cells were cultivated in
874 DMEM/10%FBS for 48 h before the experiments were started. Successful siRNA knockdown was
875 monitored by CD36 antibody staining.
876 **Cholera toxin subunit B uptake assay.** MEFs were plated on fibronectin coated glass dishes and cultivated
877 for 48 h. The cholera toxin uptake assay was performed as described by (Sotgia *et al.*, 2002). Briefly, after
878 washing twice with cold PBS cholera toxin subunit B labelled with Alexa594 was applied to the cells. The
879 treated MEFs were incubated for 30 min in the dark on ice. Afterwards the cells were washed twice with
880 PBS and incubated for 30 min with cultivation medium at 37 °C. After fixation with 4% PFA, DAPI staining
881 solution was added for 10 min. Before embedding in ImmoMount, the cells were washed PBS. Cholera
882 toxin uptake was analyzed with a Zeiss LSM700 microscope with a 63x Zeiss objective. The Alexa594
883 staining intensity was measured by ImageJ. For each experiment 10 different cells were examined.
884 **TIRF live imaging of caveolae movement.** MEFs transfected with pCav1-EGFP were incubated for 48 h on
885 fibronectin coated cover slips (25 mm diameter). Samples were mounted in Attofluor Cell Chamber
886 (Thermo) in a physiological buffer (130 mM NaCl, 4 mM KCl, 1.25 mM NaH_2PO_4-H_2O, 25 mM $NaHCO_3$, 10
887 mM glucose, 2 mM $CaCl_2$, 1 mM $MgCl_2$, pH 7.3, 305-315 mOsm/kg).
888 TIRF imaging was performed on an inverted Microscope (Nikon Eclipse Ti) equipped with a 488 laser
889 (Toptica), an dicroic mirror (AHF, zt405/488/561/640 rpc), a 60x TIRF objective (Nikon, Apo TIRF NA 1.49),
890 an appropriate emission filter (AHF, 400-410/488/561/631-640) and a sCMOS camera (mNeo, Andor). All

891 components were operated by open-source ImageJ-based micromanager software. All experiments were
892 performed at 37 °C. To investigate the movement of single caveolae transfected cells were selected in
893 which regions of individual Cav1 spots were observed (ROIs illustrated in Fig. 4J, enhanced images).
894 Recordings were obtained with the following imaging settings: image size 1776x1760 pixel, 1x1 binning,
895 500 frames, 200 ms exposure time/frame. For data analysis only the first 150 frames were investigated.
896 After cropping to the specific ROI, kymograph analysis of several positions within the ROIs were carried
897 out using the Reslice function of ImageJ/Fij. Carefully investigation of the kymographs revealed a single,
898 straight line for fixed, not moving caveolae and sparks or short lines for fast moving caveolae.
899 **Transmission Electron microscopy (TEM).** Mice were fixed by perfusion with 4% (w/v) formaldehyde in
900 0.1 M phosphate buffer and tissues were dissected to 1-2 mm^3 cubes. For morphological analysis, tissue
901 blocs were postfixed in phosphate buffered 2.5% (v/v) glutaraldehyde. Samples were treated with 1%
902 (v/v) osmium tetroxide, dehydrated in a graded series of ethanol and embedded in the PolyBed® 812 resin
903 (Polysciences Europe GmbH). Ultrathin sections (60-80 nm) were cut (Leica microsystems) and stained
904 with uranyl acetate and lead citrate before image acquisition. For immuno-labeling, samples were fixed
905 by perfusion as described above, but postfixed in phosphate buffered 4% (w/v) formaldehyde with 0.5%
906 (v/v) glutaraldehyde for 1 hour. Samples were further processed as described in Slot and Geuze (Nature
907 protocols, 2007). Briefly, samples were infiltrated with 2.3 M sucrose, frozen in liquid nitrogen and
908 sectioned at cryo temperatures. Sections were blocked and washed in PBS supplemented with 1% BSA
909 and 0.1% glycine. Labeling was performed with an anti-caveolin-1 antibody 1:500 (abcam #2910) and 12
910 nm colloidal gold (Dianova). Sections were contrasted with 3% tungstosilicic acid hydrate (w/v) in 2.8%
911 polyvinyl alcohol (w/v) (Kärgel *et al.*, 1996). Samples were examined at 80 kV with a Zeiss EM 910 electron
912 microscope (Zeiss). Acquisition was done with a Quemesa CDD camera and the iTEM software (Emsis
913 GmbH).
914 **Electron tomography (ET).** To obtain electron tomograms 250 nm slices of EHD2 del/del BAT were
915 prepared of samples embedded in resin and treated as described for TEM. The samples were tilted from
916 60 to -60° in 2° steps and examined at 120 kV with a FEI Talos electron microscope. FEI tomography
917 software was used for acquisition of tomograms, detailed analysis and reconstruction was done with
918 Inspect3D, Amira (both obtained from FEI) and IMOD (University of Colorado, USA).
919 ***In situ* hybridization.** Digoxigenin-labeled riboprobes were generated using a DIG-RNA labeling kit
920 (Roche). In situ hybridizations were performed on 14 µm cryosections prepared from E18.5 wt embryos
921 as previously described (Wilkinson, 1993). To generate an Ehd2 specific in situ probe, a 400 bp fragment
922 was amplified from wildtype cDNA using PCR and primer listed below. The PCR product was cloned into

923 pGEM-Teasy (Promega). T7 and sp6 polymerases were used to generate Ehd2-sense and antisense probes,
924 respectively.
925 EDH2_ISH_FWD: 5'-CAGGTCCTGGAGAGCATCAGC-3'
926 EDH2_ISH_REV: 5'- GAGGTCCTGTTCCTCCAGCTCG-3'
927 **Western Blot.** EHD2 protein level in different tissues was examined by Western Blot. Therefore EHD2 +/+,
928 EHD2 del/+ and EHD2 del/del mice were sacrificed by cervical dislocation and organs were dissected and
929 snap frozen in liquid nitrogen. After homogenization of the tissue in 1x RIPA buffer (Abcam) with a glass
930 homogenizer, the tissue lysate was incubated for 1 h on ice followed by 15 min centrifugation at 15,000
931 rpm. Supernatant was transferred in a fresh tube and protein concentration was measured by NanoDrop.
932 At least 10 µg protein/lane was applied to 4-12% SDS-PAGE NuPage (Invitrogen) and SDS-PAGE was
933 performed accordingly to the manufacture's protocol. Afterwards, proteins were blotted on nitrocellulose
934 membrane (Amersham) at 80 V for 1 h, followed by blocking of the membranes with 5% milk powder (in
935 TBST, 150 mM NaCl, 20 mM Tris-HCl, pH 7.5, 0.1% Tween20) for 2 h at room temperature. To detect EHD2
936 protein level rabbit-anti-EHD2 (1:2,000) was applied over night at 4 °C. After washing with TBST the
937 secondary antibody goat-anti-rabbit-HRP was added to the membrane for 2 h at room temperature.
938 Detection of EHD2 bands results from ECL detection solution and intensities were obtained by ChemiDoc
939 XRS (Biorad). Please see key resources table for all antibodies used in this study.
940 **Blood plasma analysis.** To measure distinct blood plasma parameter related to metabolic changes like
941 adiponectin, insulin or free fatty acids blood was taken from EHD2 del/+ and EHD2 del/del mice
942 immediately after cervical dislocation. All blood samples were taken at 10.00 am. Briefly, mice were
943 opened and the thorax was partly removed to get access to the left heart ventricle, a cannula was inserted
944 and blood samples were taken. After short centrifugation at high speed, the plasma fraction was
945 transferred to a fresh tube and snap frozen in liquid nitrogen. The following assays were used to measure
946 the described blood plasma markers: Plasma insulin levels were measured by Mouse Ultrasensitive Insulin
947 ELISA (80-INSMSU-E10, Alpco). Plasma adiponectin and leptin levels were measured by Mouse
948 Adiponectin/Acrp30 (DY1119) and Mouse/Rat Leptin (MOB00) ELISA kits (R&D Systems). Plasma lipids
949 were quantified with commercially available kits: cholesterol (Cholesterol liquicolour colorimetric assay,
950 Human, Wiesbaden, Germany), triglycerides/glycerol (Triglyceride/Glycerol Calorimetric Assay, Sigma)
951 and non-esterified fatty acids (Wako Chemicals). All measurements were done according to
952 manufacturers' recommendations.
953 **Fatty acid uptake assay.** EHD2 del/+ and EHD2 del/del pre-adipocytes were seeded in 6-well plates
954 (100.000 cells/well) and differentiated in mature adipocytes as described above. The fatty acid uptake

955 assay was performed as described elsewhere (Dubikovskaya *et al.*, 2014). Briefly, after 5 days of
956 differentiation, adipocytes were starved for 1 h with serum-free DMEM. Next, 2 µM dodecanoic acid
957 (FA12) labelled with BODIPY (Molecular probes #D3822) diluted in serum-free DMEM + 10 µg/ml insulin
958 was added to the adipocytes and incubated for 5, 10, 20, 30 and 60 min at 37 °C. After washing twice with
959 ice-cold PBS, 150 µl 0.25% trypsin/EDTA/PBS was applied to detach the cells. The adipocytes were treated
960 with 500 µl ice-cold FACS buffer (HBSS/10%FBS/10 mM EDTA) and the cell solution was transferred to
961 FACS tubes. Shortly before measurement, 1 µl/ml propidium iodide was added. FACS experiments were
962 performed at LSR Fortessa 5Laser with the following parameters: FSH: A, H, W, Voltage 255; SSC: A, H, W,
963 Voltage 203; A488: A, Voltage 198; PE: A, Voltage 341. For each FACS sample 30.000 cells were
964 investigated. As negative control unstained EHD2 del/+ and EHD2 del/del adipocytes were examined at
965 first and the obtained BODIPY intensity values were used as a reference for unstained cells. To exclude
966 adipocytes which did not show any positive fatty acid uptake, all unstained cells were removed resulting
967 in an only positive stained population (R1, illustrated in red in Fig. 3G and H). Within this R1 population
968 adipocytes with strongly increased BODIPY intensity values were gated to population R2 (blue, Fig. 3G, H).
969 Detailed analysis/gating and statistics was done by using FlyingSoftware2.5.1 (Perttu Terho, Cell Imaging
970 Core, Turku Center for Biotechnology). For each experiment 15.000 cells were analyzed and gated to the
971 unstained, R1 or R2 population. Next, the percentage of the cells gated to the populations were calculated
972 for every time point and illustrated in the bar graph (Fig. 3I). R2 population was investigated in more detail
973 by normalization to the R2 cell number of EHD2 del/+ adipocytes (Fig. 3J).
974 **Glucose uptake assay.** Glucose uptake of EHD2 del/+ and EHD2 del/del adipocytes was measured as
975 described by BioVison (2-NBDG Glucose uptake assay). Briefly, adipocytes were treated as described for
976 fatty acid uptake assay. However, after starvation 200 µM 2-NBDG (2-deoxy-2-[(7-nitro-2,1,3-
977 benzoxadiazol-4-yl) amino]-D-glucose, molecular probes #N13195) diluted in serum-free DMEM + 10
978 µg/ml insulin was applied to the cells followed by incubation times from 5-60 min. Staining analysis was
979 done as mentioned for fatty acid uptake with the same FACS parameters and gating procedure whereby
980 only one positive stained cell population was examined (R1, illustrated in Fig. S3A).
981 **Gene expression analysis.** EHD2 del/+ and EHD2 del/del adipocytes were differentiated for 5 days,
982 washed twice with ice-cold PBS and RNA was isolated accordingly to the Qiagen protocol (RNeasy Mini
983 Kit, Qiagen). SuperscriptIII First Strand Synthesis Kit (Invitrogen #18080051) was used to obtain
984 corresponding cDNA, which then was used for real-time PCR. Gene expression levels were analyzed by
985 GoTaq q-PCR (Promega, #A6001) Master Mix in Fast real time PCR cycler (Applied Biosystems) accordingly
986 to instructor's protocol. To measure the relative fold change of genes in EHD2 del/del adipocytes

987 compared to EHD2 del/+, the comparative real-time PCR method was applied whereby actin was used as
988 reference gene. Please see key resource table for detailed primer description.
989 Total mRNA from murine gonadal adipose tissue (gWAT) was extracted with RNeasy Mini Kit (QIAGEN
990 GmbH, Hilden) according to manufacturer's instructions. RNA was transcribed using the Moloney Murine
991 Leukemia Virus Reverse Transcriptase (M-MLV RT, Promega) according to manufacturer's
992 recommendations. Expression of mRNA was determined by quantitative real-time PCR on LightCycler 480
993 II/384 (Roche, Rotkreuz, Switzerland) using GoTaq Probe qPCR Master Mix (Promega, Madison, USA)
994 applying TaqMan Gene Expression Assays. Target gene expression of was normalized to the mean
995 expression of *Eef2*, *Ppia* and *Actb* in murine samples.
996

Gene	**Description**	**TaqMan Assay**
EHD2	EH-domain containing 2	Hs.PT.58.4969281
Ehd2	EH-domain containing 2	Self-designed
Actb	Actin, beta	Self-designed
Eef2	Eukaryotic translation elongation factor 2	Self-designed
Ppia	Peptidylprolyl isomerase A	Mm.PT.39a.2.gs

997
998 ***Actb***
999 Left primer: TACGACCAGAGGCATACAG
1000 Right primer: GCCAACCGTGAAAAGATGAC
1001 Probe: TTGAGACCTTCAACACCCCAGCCA
1002 ***Eef2* (Integrated DNA Technologies)**
1003 Left primer: CACAATCAAATCCACCGCCA
1004 Right primer: TGAGGTTGATGAGGAAGCCC
1005 Probe: TAAGCAGAGCAAGGATGGCT
1006 ***Ehd2* (UPL, Roche)**
1007 Left primer: CAGCTGGAGCACCACATCT
1008 Right primer: TCATGTGCCATCAACAGCTC
1009 UPL probe: #80
1010 **Lipid composition.** The measurement of lipid amount and its composition in tissue samples or cells were
1011 performed by Lipotype GmbH (Dresden, Germany). For this, tissue samples were homogenized

1012 accordingly to the supplied Lipotype protocol and diluted samples (1 mg/ml) were frozen and analyzed by
1013 Lipotype. MEF were split and the cell pellet was diluted in cold PBS to a final cell number of 30,000 cells/ml.
1014 **Type 2 Diabetes Knowledge Portal – *Ehd2* gene info**. Ehd2 mutations in patients suffering from T2D were
1015 investigated via the T2D knowledge portal: Type 2 Diabetes Knowledge Portal. *EHD2*.
1016 type2diabetesgenetics.org (NIH Accelerating Medicines Partnership, 2014). 2018 May 16,
1017 http://www.type2diabetesgenetics.org/gene/geneInfo/EHD2,
1018 http://exac.broadinstitute.org/gene/ENSG00000024422
1019 **Statistical analysis.** At first, a normality distribution test (Kolmogorov-Smirnov test) was carried out for all
1020 experimental values. If the data was normally distributed, Student t-Test (two-tailed P-value) was applied,
1021 otherwise Mann-Withney-Rank-Sum (two-tailed P-value) test was used to calculate the significant
1022 difference between two groups. Cav1 and CD36 staining intensities were correlated for EHD2 wt and KO
1023 MEFs (Fig. 6D) by using Pearson correlation. The correlation and the 95% confidence interval was
1024 calculated by Prism (GraphPad software). Two-way-Anova tests were used to investigate LD size after
1025 CD36 siRNA knockdown, whereby for EHD2 wt and KO MEFs each CD36 siRNA#1-3 treated cells were
1026 compared to nonsense siRNA (negative control, Fig. 6F). Box plots, if not otherwise indicated in the figure
1027 legends, always represents median with whiskers from minimum to maximum, column bar graphs and
1028 line graphs represent mean with mean standard error of the mean (SE). Statistical calculations were
1029 carried out by using Prism (GraphPad software). Distribution of LD sizes represented in histograms were
1030 also obtained by using Prism. For all experiments including the examination of mice or mouse tissue, n
1031 represents the number of mice which were used (Fig. 1, 2, 4, 7, S6, S7) and all analyzed cryo/paraffin
1032 sections or caveolae are also indicated (e.g.: n = 80 caveolae/3 mice). In cell culture experiments (Fig. 3,
1033 5, 6, S3, S4, S5), n represents the number of observed events (e.g.: lipid droplet area, staining intensity)
1034 and the number of independently performed experiments (e.g.: n = 80 lipid droplets/3 independent

1035 experiments). The following P-values were used to indicate significant difference between two groups: *

1036 $P<0.05$; ** $P<0.001$; *** $P<0.0001$.

1037